Journal of Advanced Research xxx (xxxx) xxx

Contents lists available at ScienceDirect

Journal of Advanced Research

journal homepage: www.elsevier.com/locate/jare

Original Manuscript

Chaperone-mediated autophagy sustains pericyte stemness necessary for brain tissue homeostasis

María Dolores Salinas [a,b,c], Carlos M. Martínez [d], Francisco J. Roca [b,e], David García-Bernal [b,c,f], Marta Martínez-Morga [a,c], Juan R. Rodríguez-Madoz [g,h], Felipe Prósper [g,h,i,j], Agustín G. Zapata [k], Jose María Moraleda [c,f], Salvador Martínez [l], Rut Valdor [a,b,c,*]

[a] Unit of Autophagy, Immune Response and Tolerance in Pathologic Processes, Biomedical Research Institute of Murcia-Pascual Parrilla (IMIB), 30120 Murcia, Spain
[b] Department of Biochemistry and Molecular Biology B, and Immunology, University of Murcia (UMU), 30120 Murcia, Spain
[c] Cell Therapy and Hematopoietic Transplant Group, Faculty of Medicine, UMU, 30120 Murcia, Spain
[d] Pathology Unit, IMIB, 30120 Murcia, Spain
[e] Unit of Infectious Disease Pathology, Clinical Microbiology and Tropical Medicine, IMIB, 30120 Murcia, Spain
[f] Virgen de la Arrixaca University Hospital, Hematopoietic Transplant Group, IMIB, 30120 Murcia, Spain
[g] Hemato-Oncology Program, Cima Universidad de Navarra, IdiSNA, 31008 Pamplona, Navarra, Spain
[h] Centro de investigación Biomédica en Red de Cancer (CIBERONC), Madrid, Spain
[i] Department of Dermatology and Cell Therapy, Clinica Universidad de Navarra (CUN), IdiSNA, 31008 Pamplona Navarra, Spain
[j] Cancer Center Clinica Universidad de Navarra (CCUN), 31008 Pamplona, Navarra, Spain
[k] Department of Cell Biology, Faculty of Biology, Complutense University, 28040 Madrid, Spain
[l] Instituto de Neurociencias-Miguel Hernández University (UMH-CSIC), 03550, San Juan de Alicante, ISABIAL, CIBERSAM, Alicante, Spain

HIGHLIGHTS

- Chaperone-mediated autophagy (CMA) maintains mesenchymal-like properties of pericytes.
- CMA is crucial for preserving the stemness of pericytes.
- Inflammatory mediators reduce CMA activity in pericytes.
- Reduction of CMA activity in pericytes impairs tissue repair and enhances inflammation.
- Preserving CMA in pericytes helps modulate differentiation and supports tissue repair though their secretome.

GRAPHICAL ABSTRACT

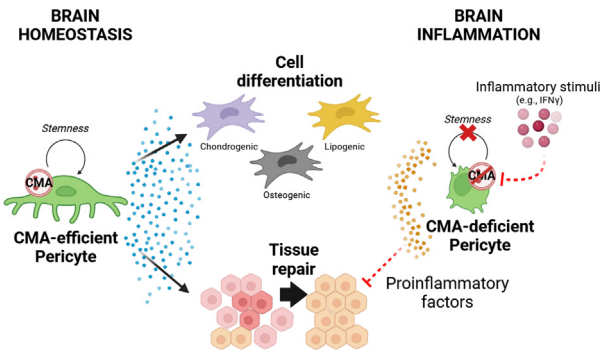

ARTICLE INFO

Article history:
Received 30 July 2024
Revised 11 April 2025
Accepted 11 April 2025
Available online xxxx

Keywords:
Chaperone-mediated autophagy
Inflammatory damage
Injury
Pericytes as functional mesenchymal stem cells

ABSTRACT

Introduction: Pericytes (PCs) are mural cells exhibiting some mesenchymal stem cell (MSC) properties and contribute to tissue regeneration after injury. We have previously shown that glioblastoma cancer cells induce in PCs, a pathogenic upregulation of chaperone-mediated autophagy (CMA) which modulates immune functions and MSC-like properties to support tumor growth.
Objectives: The aim of the study was to interrogate the role of CMA-regulated MSC properties in PCs in the context of tissue repair during inflammation triggered by a demyelinating injury.
Methods: Studies of RNA-seq were done PCs with (WT) and without (LAMP-2A KO) CMA. Cell characterization related to stemness, lineage and morphology was done in WT and KO PCs. Secretome analysis and cell differentiation assay using the supernatants from CMA-efficient and deficient PCs cultures was done in mesenchymal cells. Inflammatory response of brain cells was assessed with WT and KO PCs secretome. To corroborate *in vitro* results, CMA modulation in response to inflammation in PCs and tissue repair

* Corresponding author.
E-mail address: rut.valdor@um.es (R. Valdor).

https://doi.org/10.1016/j.jare.2025.04.015

Please cite this article as: M.D. Salinas, C.M. Martínez, F.J. Roca et al., Chaperone-mediated autophagy sustains pericyte stemness necessary for brain tissue homeostasis, Journal of Advanced Research, https://doi.org/10.1016/j.jare.2025.04.015

Secretome
IFNγ

markers were measured in the lesion areas of a demyelination mouse model and correlated with the tissue reparation after intravenous PC administration. An inflammatory mediator was used to study effects on PC-CMA activity.

Results: We found that inflammatory mediators such as IFNγ downregulate CMA in PCs, suppressing PC stemness and promoting a pro-inflammatory secretome. Restoration of PC CMA activity during inflammation maintains PC MSC properties and induces an MSC-like proteome which decreases inflammation and promotes tissue repair. We identified secreted proteins involved in regenerative and protective processes, and therefore, necessary to restore brain tissue homeostasis after inflammation induced by a demyelinating injury.

Conclusion: we show that manipulation of CMA activity in host PCs could be a useful therapeutical approach in the context of brain inflammation, which might be extended to other diseases where the pericyte has a key role in response to inflammation.

Introduction

Pericytes (PCs) are mural cells that surround endothelial cells present in capillaries, arterioles, and venules [1]. In the brain, PCs properly maintain the vascular network between the capillaries and the brain parenchyma, thereby contributing to the integrity of the blood–brain barrier (BBB) [1]. In addition, PCs regulate blood flow and vascular development, contribute to both neuroprotection and neuroinflammation, and play a role in the cell-to-cell communication between neurovascular units, consisting of microglia, astrocytes, neurons, and endothelial cells [2,3].

PCs also play a role in vascular homeostasis in the central nervous system (CNS) by regulating the non-permissive properties of the brain vasculature for leukocyte trafficking [4]. PCs show phagocytic properties and the ability to present antigens, enhance T cell homing, and act as sensors for systemic inflammation, releasing inflammatory mediators and altering the function of surrounding cells such as microglia [5–8]. In the context of degenerative diseases and vascular pathologies, activated PCs worsen the outcome by contributing to BBB disruption by a deregulated PC proliferation that leads to a lack of them in blood vessels [9–13].

It is well known that PCs share some properties with mesenchymal stem cells (MSCs) in the CNS and peripheral nervous system and show regenerative capacities in several pathologies such as ischemia–reperfusion injury [14–18], Alzheimer's disease [2,10,19], and cancer [20–22]. In recent years, increasing evidence has shown that PCs, like MSCs, contribute to tissue remodeling in response to injured/damaged tissue and vascular inflammation [23,24], representing multipotent cells capable of differentiating into different cell subtypes both *in vitro* and *in vivo* [25–27]. These findings highlight the relevance of PC function in the context of diverse human pathologies, but the mechanism by which PCs are modulated during inflammation and whether they contribute to tissue repair remains unknown.

Chaperone-mediated autophagy (CMA) is a specialized type of autophagy that targets and degrades soluble cytosolic proteins containing specific amino acid motifs (KEFRQ or KFERQ-like) in their sequence recognized by the cytosolic chaperone heat-shock cognate 71 kDa (Hsc70) [28,29]. CMA activity directly correlates with the levels of the lysosome-associated membrane protein 2A (LAMP-2A), the receptor that binds target proteins, having a key role as a limiting step in this pathway [30,31]. Physiologically, this activity is vital for preserving tissue homeostasis by selectively promoting the cell clearance of pathogenic proteins, such as oxidized or damaged proteins. Moreover, CMA plays a critical role in modulating cellular proteostasis by selectively degrading functional proteins implicated in cell metabolism, differentiation, and survival [32–36] and its activity is strongly increased under cellular stress [37–40], disrupting normal physiological functions. In contrast, its failure due to aging, or its dysregulation by pathological processes, increase the susceptibility to suffering from diseases, including cancers, neurodegenerative diseases and inflammatory disorders [41–55].

CMA activity has recently been reported to be a critical contributor to pluripotency of embryonic stem cells [56], and to maintain hematopoietic stem cell (HSC) function through protein quality control and adequate energy supply throughout the lifespan [57]. This selective autophagy process has been found to be a key mechanism in stem cell pluripotency control through epigenetic, transcriptional, and differentiation regulation [35,58,59]. Intrinsic CMA activity in cancer stem cells is essential for their maintenance [60,61], and it is aberrantly upregulated by cancer cells in multipotent PCs to modulate the immune and MSC-like properties that support tumor growth and survival [21,62]. We have recently shown that CMA-defective PCs can eliminate glioblastoma (GB) tumor cells [63], and we hypothesized that, as in cancer, PCs could modulate CMA activity as well as functions typical of MSCs (MSC-like) in response to inflammation in damaged brain tissue [63]. Elucidating and understanding how inflammation modulates PC function in the context of tissue damage will help to find new therapeutic approaches for pathologies associated with tissue repair during inflammation where PCs play an important role as mural MSC-like elements.

Here, we show that CMA activity deeply impacts the gene expression profile and thus the secretome in PCs: lack of homeostatic CMA levels in response to inflammatory stimuli decreases expression of genes related to stemness which abrogates PC MSC-like functions and induces a differentiated pro-inflammatory phenotype. Studying the cellular response to inflammation in a demyelinating mouse model we have discovered that the secretome of PCs modulates stemness properties of surrounding MSC-like PCs in the brain tissue. Demyelination-mediated inflammation impairs CMA activity in resident PCs which induces a pro-inflammatory phenotype and inhibits brain tissue regeneration. We have found that intravenous administration of brain PCs with efficient CMA reduces inflammation and induces tissue regeneration, which correlates with LAMP-2A expression, and thus CMA activity, in host PCs after brain injury. Thus, prevention of CMA loss in host PCs in response to tissue inflammation leads to the maintenance of MSC-like functions of PCs and a functional secretome required for tissue repair.

Altogether, our findings indicate that CMA, a ubiquitous cellular mechanism to maintain cell homeostasis, could be targeted in host PCs in the context of tissue inflammation and repair. Indeed, manipulation of the secretome-mediated MSC-like function of PCs by modulating CMA activity represents an attractive approach for the development of new therapies for other inflammatory diseases beyond cancer.

Materials and methods

Mice

Male and female mice of six to eight weeks-old C57BL/6-Tg (ACTB-EGFP)1Osb/J and WT C57BL/6 (Charles River Laboratories) were maintained under specific pathogen-free (SPF) conditions in the animal facilities of the University of Murcia and of the Institute of Biomedical Research of Murcia (IMIB), respectively. All animal procedures were approved and performed according to the guidelines set by the Institutional Animal Care and Use Committee of the University of Murcia (approved protocol A13150201) and of the IMIB (approved protocol A13210202).

Pericytes isolation and culture

Primary brain PCs (WT PCs and GFP-PCs) were isolated from mice according to the method of Oishi et al. [64] as described previously [21,65]. Briefly, mouse brains were extracted and dissociated. The tissue was then incubated with 1 mg/mL collagenase and 15 μg/mL DNase I in 10 mL Dulbecco's modified Eagle's medium (DMEM high glucose; Gibco) at 37 °C for 30 min with gentle stirring. The suspension was diluted to inactivate the digestion, centrifuged, and resuspended in DMEM containing 20 % bovine serum albumin. After centrifugation, the pellet was digested again with the same concentrations of collagenase and DNase I for 30 min. The cell suspension was centrifuged and washed, and the pellet containing the microvessel-enriched fraction was collected and expanded until 5th passage where just pericytes are remaining [65] (please see Supplementary Methods). PCs were used from the 5th to 8th passage. PCs with impaired CMA (KO PCs), were isolated from brains [21,63] of Lamp2a$^{-/-}$ mice [45].

To obtain cell supernatants for the secretome assay, cell culture media obtained from 72 h cultures of WT and KO PCs was concentrated using Amicon Ultra centrifugal filters 10 k (Millipore) and used 10 times diluted as described previously [21]. GFP-expressing PCs were used for cell tracking as described previously [21,63].

Cultures of WT and KO PCs were treated with 20 ng/mL murine IFNγ (BD Biosciences) for different time points. For immunoblotting and gene expression analysis, 0.5×10^6 WT and KO PCs were cultured in 6-well plates. Total protein lysates were obtained after 24 and 48 h and mRNA was collected after 24 h.

For morphometric analysis, images from both WT and KO PCs cells, after 120 h of culture, were acquired with a Motic AE2000 Trinocular Microscope with a Moticam 3+ camera (Motic) and the Motic Images Plus 3.0 software (Motic). The cell surface area was analyzed by measuring the perimeter (the length of the outside boundary) of the selected cells using ImageJ software (NIH, USA).

Proliferation assay

WT and KO PCs (5×10^4) were cultured in 24-well plates for 24 to 120 h. Then, both PCs were trypsinized and counted using an inverted fluorescence microscope (Nikon, Tokyo, Japan). Cell proliferation was measured by calculating the cumulative population doubling (CPD), which refers to the number of times that cell numbers have been doubled. CPD level was calculated using the formula:

$$PD = \left(\frac{1}{Log10^2}\right) xLog10\left(\frac{Nt}{N0}\right)$$

where N_0 is the number of viable cells (as determined by trypan blue exclusion) at seeding, whereas N_t is the number of viable cells at harvest.

Mesenchymal stem cell isolation and cell cultures

Mesenchymal stromal vascular fraction from murine adipose tissue (adMSCs) was isolated and cultured with the same method as described above for brain PCs purification, based on the isolation of the first adherent fraction in the culture of perivascular cells from venules and arterioles and the expansion until 5th passage where just MSCs are remaining [66,67].

Dissociated cell cultures of human periodontal ligament stem primary cells (PDLSCs), isolated and characterized by Bueno et al. [68,69], were used at the 4th-5th passage of cell culture in basal medium composed of α-MEM supplemented with 10 % serum (Sigma), 100 units/mL penicillin–streptomycin (Sigma), 50 mg/mL L-ascorbic acid (Sigma), and 2 mM L-glutamine (Sigma) at 37 °C in 5 % CO_2.

Murine microglial cell line BV2, kindly provided by Dr. Jose P. Lopez Atalaya [70], and human endothelial cell line EAhy926, kindly provided by Dr. Sonia Águila Martínez [71], were both cultured in DMEM high glucose (Biowest) supplemented with 10 % FBS (Hyclone), 1 % penicillin–streptomycin (Sigma) and 1 % Glutamax (Gibco).

Differential expression analysis, heatmap, functional annotation, and pathway analyses

Differentially expressed genes (DEGs) in PCs presenting CMA (WT PCs) and CMA-deficient PCs (KO PCs) from raw data used for the previous study [63] and publicly available in the European Nucleotide Archive ENA (*ENA* PRJEB48545) were detected using DESeq2 v1.18.1 package [72] in R computing platform v3.4.4 [73] as described previously [63]. DEGs were computed using batch correction in the formula design (design = ~condition + sample_batch). Genes with FDR Adj. $p < 0.01$ were considered significantly differentially expressed.

Network visualization of Gene Ontology enrichment of proteins of the main affected upregulated or downregulated pathways in KO PCs vs WT PCs was performed by STRING v11.5 functional protein association networks. Major clusters are circled, and node size indicates the number of proteins per node. A heatmap was generated to confirm the expression values of the most up-regulated genes related to stemness in WT PCs vs KO PCs with FDR < 0.01. To generate the heatmap, the heatmap.2 function of the R (R Core Team, 2021) gplots package was used.

Real-Time PCR (qPCR)

RNA was isolated using the RNeasy Mini Kit using manufacturer instructions. cDNA was synthesized from total RNA, and gene expression was analyzed by real-time PCR using SYBR Green in a QuantStudio 5 qPCR System (Applied Biosystems), as described previously [65]. The primer sequences are listed in Table S2. Each sample was measured in quadruple and expression levels were normalized to *Actb* and *Hprt1* expression as the housekeeping reference. The $2^{-\Delta\Delta Ct}$ method was used to determine the relative gene expression.

Cell treatments and differentiation

For osteogenic, adipogenic, and chondrogenic differentiation, 5×10^4 mouse WT and KO PCs were cultured in 24-well plates for 14 days. Cells were fixed with 4 % paraformaldehyde (PFA) for 20 min before staining. Osteogenic differentiation was assessed by Alkaline Phosphatase (ALP) staining. SIGMAFAST™ BCIP®/NBT (Sigma-Aldrich, B5655) tablets were dissolved according to the manufacturer's instructions. Cells were incubated with the substrate solution and rinsed in distilled water to remove non-

specific staining. Lipogenic lineage was identified by the detection of neutral lipid accumulation with Oil Red O (Sigma-Aldrich, O1391) staining. After fixation, cells were covered with the working solution and washed with distilled water. Chondrogenic differentiation was revealed by Alcian Blue (Sigma-Aldrich, B8438) staining, which detects the synthesis of acidic glycosaminoglycans. 1 % Alcian Blue in 3 % acetic acid, pH 2.5, was added to cells and removed with distilled water. Images of the cells were acquired using a Nikon Eclipse Ti inverted microscope. Positive cells were quantified relative to the total number of cells per field in, at least, four fields.

Staining was extracted from the cells to measure the absorbance of the dye in triplicate to a 96-well plate using a Synergy Mx plate reader (BioTek). For ALP staining, cells were lysed with PBS with 1% Tween-20 and the absorbance was measured at 670 nm. Isopropanol was used to extract the oil red stained lipid droplets, and the absorbance was measured at 492 nm. For the extraction of alcian blue stain, cells were incubated with guanidine hydrochloride (6 M) and the absorbance was measured at 600 nm.

Secretome analysis

Differential levels of secreted proteins in WT PCs and KO PCs were qualitatively analyzed, identifying the proteins related to pro-regenerative or pro-inflammatory mechanisms and according to Biological Processes of Gene Ontology through QuickGo [74,75]. For previous sample preparation, secretome protein identification, and analysis by HPLC/MS system, we followed the methods previously described [63].

Experimental parameters for HPLC and Q-TOF were set in MassHunter Workstation Data Acquisition software (Agilent Technologies, Rev. B.08.00) for free label quantification and identification [76] in three pooled of concentrated supernatants from both experimental lines (WT PCs; KO PCs) and the proteins in control cell culture media were used as negative control. KO PC and WT PC protein ratio was determined. The threshold was set at log2FoldChange $\geq$ 2.00 for enriched proteins in WT PCs, and Log2FoldChange $\leq$ $-$ 2.00 for enriched proteins in KO PCs, following other author recommendations [77]. A Venn diagram was generated with R to visualize common and distinct identified proteins between WT and KO PC secretome.

Functional secretome assays

5×10^4 PDLSCs were incubated with WT or KO PCs concentrated supernatants, or concentrated cell culture media (vehicle) for 2 weeks. No other differentiation-inducing reagent or supplement was added to the medium. Media with PC secretome was changed after 7 days of culture. Perlecan (5 μg/mL; Origene #TP762044) and follistatin (500 ng/mL; Thermofisher #120–13), alone or combined, were added every 3 days for 7 days. After 14 days, cells were collected for RNA or fixed for cytochemistry analysis for osteogenic, chondrogenic, and adipogenic differentiation.

To test the secretome anti-inflammatory properties, 2×10^5 cells of the microglial cell line BV2 were activated with 1 μg/mL lipopolysaccharide (LPS; Sigma-Aldrich) for 24 h. LPS-activated cells were incubated with WT or KO PC concentrated supernatants, or cell culture media concentrated (vehicle) for 24 h and 48 h after activation. Resting cells were used as control.

ELISA

Mouse TNF-α (Bio-Techne R&D Systems, MTA00B) and IL-1β (Bio-Techne, R&D Systems, MLB00C) levels secreted by microglial cells in the media were measured by sandwich ELISA with specific anti-mouse antibodies following the manufacturer's recommendations.

Induction of demyelinating lesion and PC administration

Lysolecithin, a membrane-solubilizing agent that exhibits specific toxicity toward myelinating cells [78,79], was used to induce a demyelinating lesion in the parietal cortex of mice. Eight-week-old WT C57BL/6 mice were injected with 5 μL of 2 % lysolecithin solution (Sigma-Aldrich) in Hanks' Balanced Salt Solution (Gibco), as described previously [80,81]. After isoflurane anesthesia, mice were placed in the stereotaxic frame (RWD Life Science) and a craniotomy was performed in the parietal cortex (1-mm from the midline and 2-mm lateral to bregma) using a microdrill (RWD Life Science). Lysolecithin was injected at a flow rate of 0.5 μL/min in the hippocampus (penetrating dorsoventrally from the brain pial surface 1.5 mm) using a 10 μL Hamilton 26G syringe mounted on a Quintessential Stereotaxic Injector (Stoelting Co.). After injection, the needle was left in place for 4 min before slowly retracting and closing the wound.

Ten days post-lesion, mice were treated with WT/KO-PCs or GFP-PCs (isolated from C57BL/6-Tg (ACTB-EGFP)1Osb/J mice) to compare to those untreated and control mice. Twelve mice were injected intravenously into the tail vein (IV therapy: 0.5×10^6 cells per mouse in 200 μL) with GFP, WT or KO PCs isolated from the brain, and compared to five control mice treated with adMSCs, five untreated mice and five intact controls. Twelve control and twelve injured mice that were intravenously treated with GFP-PCs or GFP-adMSCs were sacrificed after 3–10 days to keep track of cells as we previously described [63]. For detailed PC tracking, please see supplementary methods. Twenty-one days after therapies, mice were sacrificed, and brains were fixed in 4 % buffered formalin (Panreac Quimica). All described procedures were repeated three times.

Immunohistochemistry, immunofluorescence, and microscopy

Fixed brains were paraffin-embedded and processed by the Pathology facility (IMIB Virgen de la Arrixaca) as described previously [21]. Three-micrometer thick serial sections were obtained from paraffin-embedded samples using an automatic rotary microtome (Thermo Scientific). Sections were incubated overnight at 4 °C with the following primary anti-mouse antibodies: mouse anti-MBP (Sigma-Aldrich, NE1019), rabbit anti-BDNF (Invitrogen, PAS-85730), rabbit anti-Caspase-3 (Cell Signaling, 9662), goat anti-Iba-1 (Abcam, ab5076), rat anti-CD68 (AbDserotec, MCA1957T), rabbit anti-IFNγ (Bioss, bs-0480R), rabbit anti-Laminin (GeneTex, GTX101127) and rabbit anti-CD3 (Dako, A0452229). Sections were then incubated with their respective secondary HRP or alkaline phosphatase (ALP)-labeled polymer system (Vector ImmPress, Vector Laboratories). Finally, the immunoreaction was revealed by using a 3–3́Diaminobencidine (DAB) or (ALP) substrate kit (Dako DAB substrate kit and Vector Red Alkaline Phosphatase kit, respectively) which identifies positive immunoreaction as a dark brown (DAB) or light red (ALP) precipitate. Finally, sections were counterstained with Mayer's hematoxylin (Carlo Erba Reagents, LLG06272066). An automatic digital slide scanner (Pannoramic MIDI II-3DHistech) was used for acquisition of images.

For fluorescent double labelling, mouse anti-alpha-smooth muscle actin (α-SMA; Abcam, ab7817), goat anti-platelet derived growth factor receptor beta (PDGFRβ; R&D Systems, BAF1042), or rat CD146-APC (Miltenyi Biotec, 130–118-408) antibodies were used in combination with rabbit anti-LAMP-2A (Invitrogen, 51–2200) antibody. Labelling was visualized by fluorescence microscopy using the corresponding secondary antibody conjugated to

AlexaFluor488 (Invitrogen) or Cy5 (Invitrogen). Fluorescence samples were counterstained with DAPI (Invitrogen) prior to mounting with Mowiol. A TCS-SP8-MP-AOBS laser scanning spectral inverted Confocal Microscope (Leica Microsystems) was used to analyze the histological sections. Maximum-intensity projection of images was achieved with LAS X software (Leica Microsystems) and ImageJ software (NIH, USA). Quantification of cells was performed using ImageJ (NIH, United States) software by measuring the number of pixels per brain or the number of positive cells around the injured areas in at least, four fields.

Immunoblotting

Total cellular lysates were prepared using RIPA buffer (1 % Triton-X 100, 1 % sodium deoxycholate, 0.1 % SDS, 0.15 M NaCl, 0.01 M sodium phosphate, pH 7.2). Lysates were clarified by centrifugation and the protein concentration of the supernatant fraction was determined by a Bradford assay (Sigma-Aldrich, B6916). Primary antibodies used were rabbit anti-mouse LAMP-2A (Invitrogen, 51–2200), mouse anti-human LAMP2 (H4B4; Abcam, ab25631), rat anti-mouse iNOS (Invitrogen, PA5-17106), rabbit anti-mouse COX-2 (Cell Signaling Technology, 12282), rabbit anti-mouse α-Tubulin (Abcam, ab4074) and anti-β-actin (Santa Cruz Biotechnology, sc-47778). The blotting membranes were developed with chemiluminescent reagents (Cytiva Lifesciences, RPN2232) according to the instructions provided by the manufacturer. Quantification was performed using ImageJ (NIH, United States) software.

Transfections and CMA reporter assay

All plasmid transfections were done using Lipofectamine 2000 (Invitrogen). For CMA activity assay, 2×10^4 WT PCs were cultured in 24 well-plates and transfected with the plasmid KFERQ-PA-mCherry [82]. Twenty-four hours post-transfection, cells were exposed to 405 nm light immediately following treatment with IFNγ to photoactivate PA-mCherry. PCs were collected at 24 h after activation, fixed with 4 % PFA, and changes in the numbers of lysosomes highlighted by the reporter were analyzed by fluorescence microscopy. Images were acquired with a Nikon Eclipse Ti microscope equipped with a with 60 × Plan Apo Vc objective (numerical aperture, 1.40) and a digital Sight DS-QiMc camera (Nikon) and 387 nm/447 nm, 543 nm/593 nm filter sets (Semrock), and the NIS-Elements AR software (Nikon). CMA activity was measured as the number of fluorescent puncta per cell. Quantification was performed using ImageJ (NIH, United States). All determinations were performed in at least three experiments.

For LAMP-2A-mediated restoration of CMA, 5×10^5 WT PCs were transfected with human LAMP-2A fused to mCherry fluorescent protein and cloned in pcDNA3.1 plasmid (GenScript). After 24 h post-transfection, murine IFNγ (20 ng/mL) was added and 24 h later, human LAMP-2A expression was confirmed by immunoblotting comparing to control cells transfected with a backbone plasmid expressing mCherry.

Statistical analysis

Differences between groups were analyzed by one-way ANOVA followed by Tukey-Kramer multiple comparisons post-test. Comparisons between data pairs were analyzed using an unpaired two-tailed Student's *t-test*. Statistical significance was defined as $p < 0.05$ and indicated as $^{*}p < 0.05$, $^{**}p < 0.01$, $^{***}p < 0.001$, $^{****}p < 0.0001$ or ns for no significance. Analysis was done with GraphPad Prism (version 8.3.0).

Results

Intrinsic CMA activity in PCs is required to maintain their MSC-like properties

To interrogate putative molecular pathways modulated by CMA at baseline in PCs we compared the transcriptome of LAMP-2A-deficient PCs, completely lacking CMA activity (KO PCs), to wild-type PCs (WT PCs) (*ENA* PRJEB48545) [63]. Differentially expressed genes (DEGs) were analyzed by Gene Ontology enrichment to determine the affected biological pathways (Fig. 1A). Kyoto Encyclopedia of Genes and Genomes (KEGG) pathway enrichment analysis revealed genes involved in cell differentiation as the most upregulated in CMA-deficient PCs (Fig. 1A, left panel), suggesting that CMA activity is preventing cell differentiation and thus promoting stemness properties in PCs. In accordance with our previous findings of CMA-deficient PCs exerting anti-tumoral properties against GB cells [63], DEGs related to immune/inflammatory responses were also upregulated (Fig. 1A, left panel). Importantly, the most downregulated pathways in PCs in absence of CMA were those related to developmental processes (Fig. 1A, right panel). Finally, the assessment of the network of CMA-regulated pathways in PCs showed that cell communication and cell adhesion pathways were downregulated in the absence of CMA (Fig. 1A, right panel).

We have previously shown that CMA regulates immune responses in brain PCs [21] (Fig. S1). Furthermore, we and others have found that MSC-like properties of PCs support GB tumor growth [22,62]. Then, we next asked whether CMA-regulated MSC-like properties in PCs could be of relevance for regenerative treatments in the context of other diseases [23,24]. We assessed downregulated DEGs related to stemness (e.g., *Fzd5*, *Fzd8*, *Wnt6,* or *Fgfr3)* [83–88] in pathways involved in developmental processes (Fig. 1A, right panel) and corroborated their increased expression in WT PCs (Fig. 1B). We validated the expression of those genes by qPCR as well as other identified genes in upregulated DEGs, specifically overlapping in cell differentiation and inflammatory response (Fig. 1A, left panel). We found a fifty percent reduction of all tested genes related to stemness while genes involved in differentiation were upregulated in KO PCs (Fig. 1C) [89]. Moreover, our findings supported that reduced levels of LAMP-2A expression, and therefore of reduced CMA activity, correlated with the disappearance of PC stemness phenotype (Fig. S2). Furthermore, we found that the multipotent lineage commitment of CMA-deficient PCs was affected in absence of CMA, as most cells were differentiated to a lipogenic lineage after 3 days of culture (T3) (Fig. 2). This correlates with an expression upregulation of the lipogenic genes *Fabp4*, *Pparg* and *Ptgs1*, showing levels at least three times higher than in WT PCs (Fig. 1C). Importantly, while WT PCs still maintained their stemness in most cells after 14 days of culture (T14) (Fig. 2A-D), CMA-deficient PCs spontaneously changed their predominant cell lineage, showing increased alkaline phosphatase activity, which is associated with osteogenic differentiation (Fig. 2 A, B, and Fig. S3). In addition, KO PCs did not show significant differences in the chondrogenic staining but lost the lipogenic staining compared to WT PCs at larger times of culture (T14) (Fig. 2A, B and Fig. S3). As KO PCs initially showed a phenotype towards a lipogenic lineage (Fig. 1C and A, B), we corroborated that they were not initially differentiated to another cell lineage (Fig. 2C). Interestingly, the expression of *Axl*, a tyrosine kinase receptor implicated in the modulation of osteogenic differentiation [90,91], was significantly increased twofold, whereas the expression of the osteogenic gene *Spp1* was decreased by a third (Fig. 2C). Thus far, these results indicate that CMA might control the regulation of the osteogenic differentiation in PCs. Accordingly,

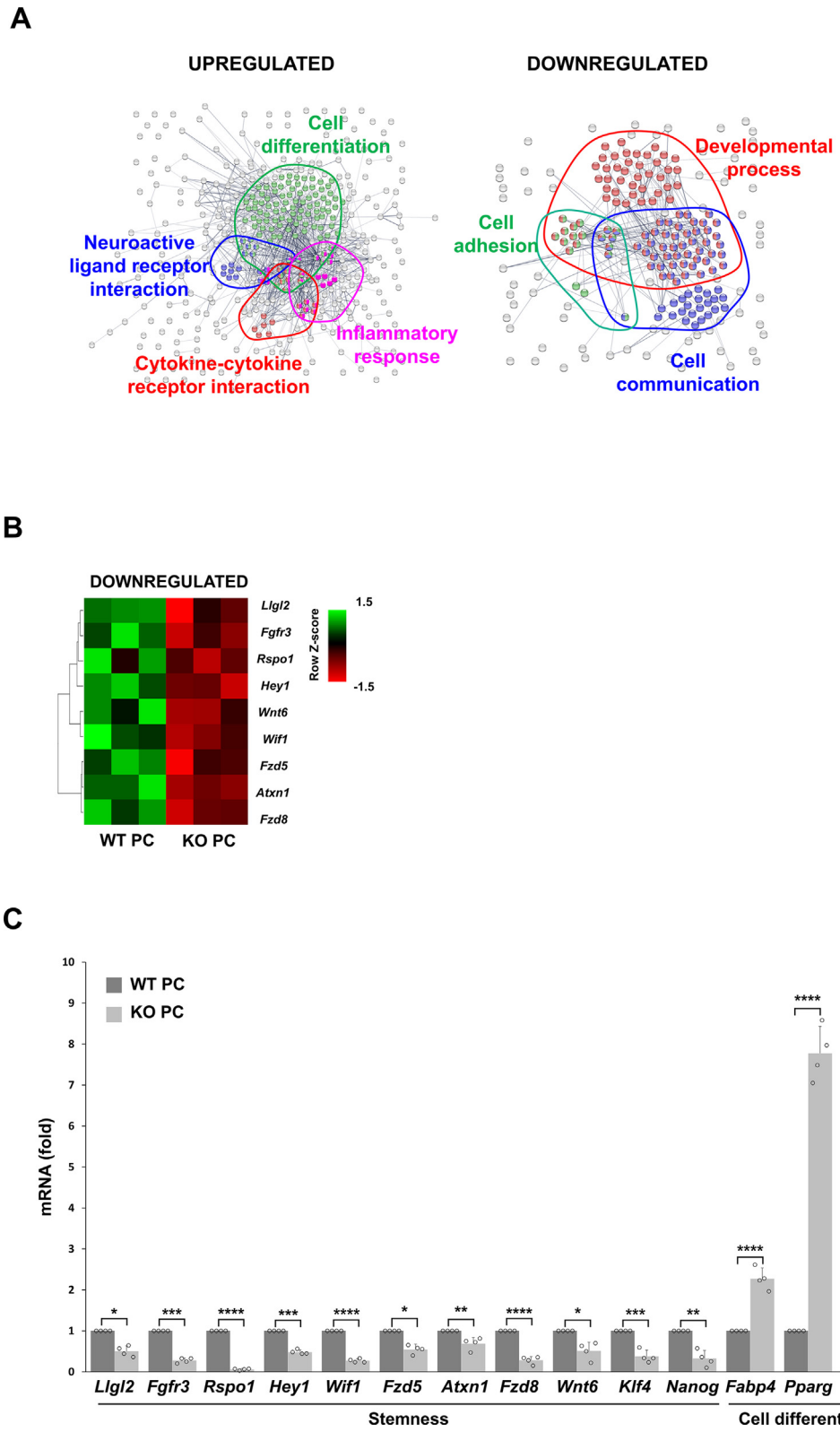

Fig. 1. CMA maintains the stemness gene pattern in PCs. (**A**) Network visualization of Gene Ontology enrichment of proteins of the main selected affected upregulated (on the left) or downregulated (on the right) pathways from CMA-dependent DEGs in CMA-deficient PCs (KO). Major clusters are encircled, and node size indicates the number of proteins per node. (**B**) Heatmap of downregulated CMA-dependent DEGs corresponding to the affected pathway related to stemness, in the main affected developmental process of KO PCs compared to WT PCs. Red boxes represent downregulated genes, and green boxes represent upregulated genes. The value of expression intensity is based on the gene expression level analysis. All previous data were obtained from three RNA pools for each experimental line of at least five independent experiments. (**C**) Validation and quantification of the mRNA expression by qPCR, of some downregulated genes that were identified in the downregulated pathway related to stemness and some upregulated genes related to cell differentiation from CMA-dependent DEGs. Data show specifically the gene expression levels in KO PCs (relative to PC basal levels) and compared to WT PCs. Each sample was measured in quadruple and expression levels were normalized to *Actb* and *Hprt1* expression as the housekeeping reference gene expression. All data represent mean ± SD obtained from at least, five experiments represented as dots, independently; *$p < 0.05$; **$p < 0.01$; ***$p < 0.001$; ****$p < 0.0001$ (Student's *t*-test). (For interpretation of the references to colour in this figure legend, the reader is referred to the web version of this article.)

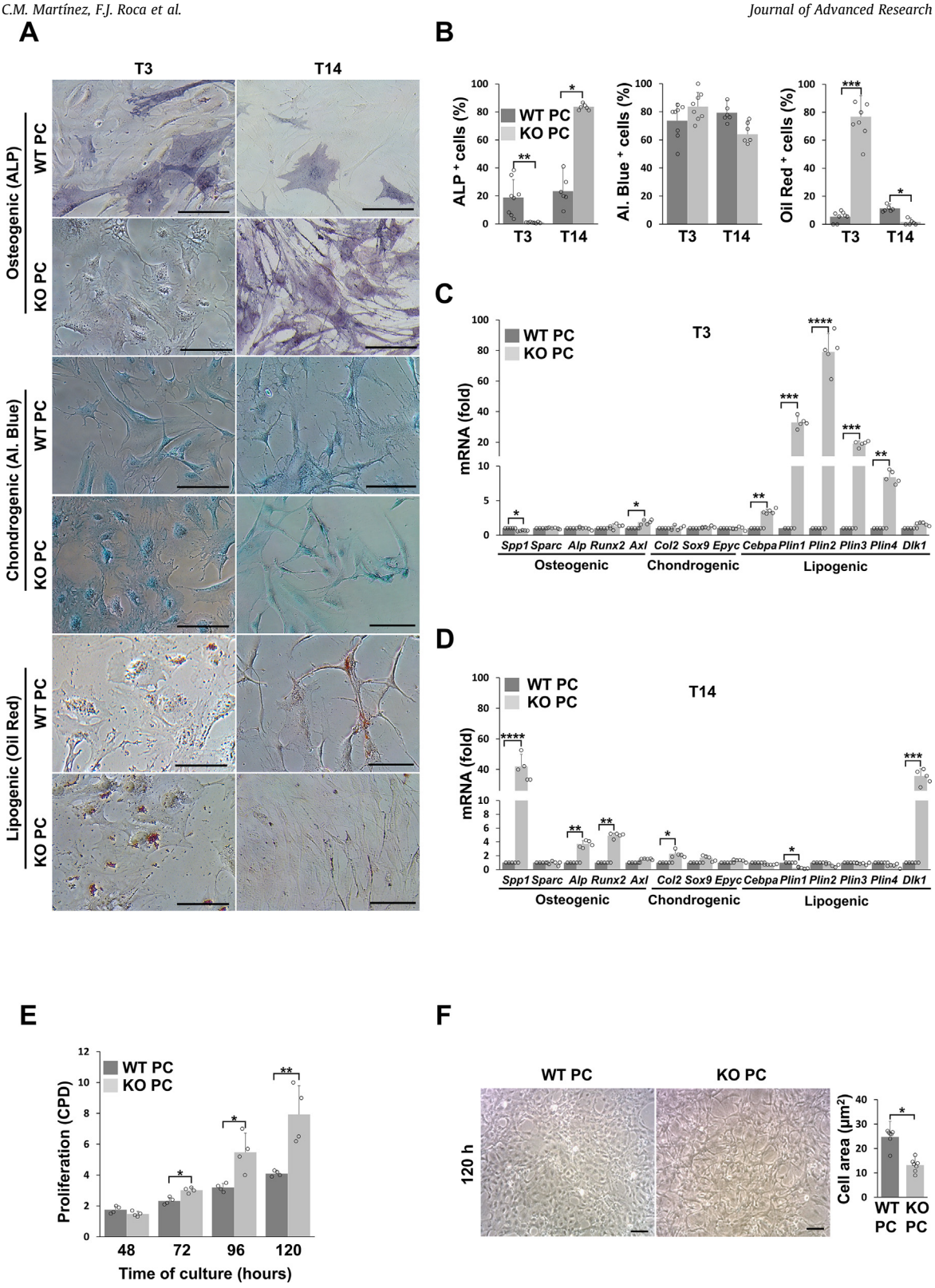

Fig. 2. CMA maintains multipotent cell properties of PCs. (**A**) Representative images of the differentiation of WT and KO PCs after 72 h (T3) and 14 days (T14) of culture. PCs are multipotent cells that can differentiate spontaneously into different lineages. Osteogenic lineage shows positive cells for alkaline phosphatase (ALP); chondrogenic lineage are positively stained cells by alcian blue (Al. Blue); and lipogenic lineage shows Oil Red O positive cells. Scale bar: 100 µm. (**B**) Graphs represent the quantification of levels of positive cells for ALP activity, Alcian Blue, and Oil Red O staining. All data represent mean ± SD obtained from at least five experiments represented as dots, independently; $^{*}p < 0.05$ (Student's *t*-test). (**C, D**) Validation and quantification of the mRNA expression by qPCR, of some genes related to osteogenic, chondrogenic and lipogenic differentiation in WT PCs or KO PCs after (**C**) 72 h (T3) and (**D**) 14 days (T14) of culture expressed as folds over WT PCs. Each sample was measured in quadruple and expression levels were normalized to *Actb* and *Hprt1* expression as the housekeeping reference gene expression. All data represent mean ± SD obtained from at least, four experiments represented as dots, independently; $^{*}p < 0.05$; $^{**}p < 0.01$; $^{***}p < 0.001$; $^{****}p < 0.0001$ (Student's *t*-test). (**E**) Cell proliferation represented as cumulative population doubling (CPD) at different time points of culture. CPD analysis was done determining viable cells by trypan blue exclusion. All data represent mean ± SD obtained from at least three experiments represented as dots, independently; $^{*}p < 0.05$; $^{**}p < 0.01$ (Student's *t*-test). (**F**) Representative images of cells after 120 h of culture showing different size quantified as cell area (µm^2). All data represent mean ± SD obtained from at least four fields per experiment in three independent experiments represented as dots; $^{*}p < 0.05$ (Student's *t*-test). Scale bar: 100 µm. (For interpretation of the references to colour in this figure legend, the reader is referred to the web version of this article.)

KO PCs showed upregulation of osteogenic genes (*Spp1*, *Alp,* and *Runx2*) and downregulation of lipogenic genes expression (*Cebpa, Plin 1, Plin 2, Plin 3, Plin4*) after 14 days of culture (Fig. 2C, D). Supporting these results, *Dlk1* gene expression, a negative regulator of lipogenesis [92–94] was highly upregulated. Altogether, our results indicate that CMA regulates PC multipotency, which maintains PC stemness, in a cell-autonomous fashion.

Neither the neural stem/progenitor cell marker nestin, that distinguishes type II from type I PCs [25,26] nor typical proteins of the extracellular matrix (ECM) implicated in tissue remodeling [95,96] showed significant differences in presence or absence of CMA activity (Fig. S4). However, our findings on the loss of expression of genes related to stemness and cell lineage in KO PCs (Figs. 1 and 2), were accompanied by changes in other MSC-like properties (Fig. 2E, F and Fig. S5). We found that PCs increased their proliferation by five times and reduced their size by fifty percent after 3 days of culture (Fig. 2E, F). Additionally, CMA-deficient PCs showed different expression of hypoxia-inducible factor-1 alpha (HIF-1α) (Fig. S5A), a well-known CMA substrate [38], which suggest the occurrence of metabolic changes [12,97,98]. The epithelial-mesenchymal transition markers (EMT) E-cadherin, N-cadherin, and occludin are implicated in PC adhesion for vascular stabilization [99]. Although the percentage of cells expressing these markers was not significantly affected in CMA-deficient PCs compared to controls, their expression levels per cell was fifty percent reduced (Fig. S5B), corroborating the requirement of CMA activity to regulate cell adhesion pathways (Fig. 1A). Thus far, our results corroborated that CMA is essential to maintain the MSC-like properties of PCs.

CMA activity in PCs is required to maintain a functional MSC-like secretome

Could CMA-driven PC MSC-like properties and secretome have modulatory effects on the stemness functions of other PCs or other cells with stem-like properties needed for tissue repair? To answer this question, we analyzed the effect of the secretome from both WT and CMA-deficient PCs in the differentiation of human periodontal ligament stem cells (PDLSCs), which derive from the neural crest as brain PCs [100–103]. PDLSCs showed a clear osteogenic commitment after 14 days of culture (Fig. 3A, B and Fig. S6). This differentiation was inhibited when they were cultured with the supernatants (conditioned medium) from WT PCs; however, supernatants from CMA-deficient PCs failed to promote this inhibition (Fig. 3A, B and Fig. S6). In contrast, PDLSCs cultured with WT PC supernatants maintained their chondrogenic lineage (Fig. 3A, C). We did not see differences when we assessed adipogenic differentiation (Fig. 3A, D). Accordingly, we found that osteogenic gene expression in differentiated PDLSCs was significantly reduced by half in PDLSCs cultured with the media from WT PCs (Fig. 3E). These results indicate that CMA activity in the PC is critical to maintain a proper MSC-like secretome which could directly orchestrate cellular functions during tissue regeneration.

Thus, PC stemness might be dependent on CMA activity through a functional secretome containing regulators responsible for stemness function on surrounding cells and thus, affect tissue repair and regenerative processes. To determine if this was the case, we performed proteomic analyses to identify the most abundant proteins secreted by WT PCs compared to KO PCs (Table 1). We found a deficient protein secretion in CMA-deficient PCs compared to WT PCs, with 10 differentially expressed proteins that were absent in KO PC cultures (Fig. 3F and Table S1). Interestingly, this analysis showed only 3 proteins differentially expressed in CMA-deficient PCs compared to WT PCs. Excitingly, several functional groups associated with tissue repair and regenerative processes were identified in the WT condition, whereas KO PCs differentially presented groups of proteins implicated in inflammatory response and lipid metabolism (Fig. 3G and Table 1). Thus, according to Biological Processes of Gene Ontology, 12 proteins were identified as molecules that may be preferentially secreted by WT PCs and related to tissue development and cell differentiation mechanisms, such as UHRF1 (ICBP90)-binding protein 1 [104–107], follistatin-related protein 1 [108–110] and SPARC [111–114]; 9 to wound healing, such as plasminogen activator inhibitor 1 [115–117] and perlecan [118–121]; 9 to extracellular matrix organization such as beta-actin-like protein 2 [122]; and 5 to angiogenic processes, such as antithrombin III [115,123,124]. Conversely, different protein fractions associated with extracellular matrix assembly (4 proteins), inflammatory response (3 proteins), and lipid metabolism (2 proteins) were identified in the secretome of KO PCs, including dipeptidyl aminopeptidase-like protein 6 [125–128] and long-chain-fatty-acid-CoA ligase [129] (Fig. 3G and Table 1).

Thus, our results shed light on possible mechanisms by which PCs need CMA activity to maintain a regulated secretome functionally equivalent to that of MSCs, including proteins involved in tissue repair and regeneration. Furthermore, we found secreted proteins enriched in WT PCs involved in anti-inflammatory processes such as antithrombin [124], the tissue protector myokine follistatin [110], apolipoprotein A-I [130], the plasminogen activator inhibitor 1 [117] and the UHRF1 (ICBP90)-binding protein 1 [107], supporting that a secretome dependent on CMA activity promotes anti-inflammation.

Importantly, we confirmed the functional effects of some of these proteins on PDLSCs differentiation, such as follistatin (FLT) and perlecan (PLC), which significantly prevented the osteogenic differentiation of PDLSCs after 14 days of culture (Fig. 4A-E), maintaining their stemness with a higher synergic effect between both proteins added to the cultures (Fig. 4A, B and Fig. S6B). Moreover, our results showed the anti-inflammatory properties of the CMA-dependent secretome of PCs. The WT supernatant addition to activated microglia cells significantly ameliorated at least three times the expression of pro-inflammatory genes (Fig. 4F) and the secretion of pro-inflammatory cytokines such as TNF-α (Fig. 4G) and IL-1β (Fig. 4H), compared to activated microglia incubated with the control media (vehicle) or the KO PC supernatants. Additionally, these findings were supported by the clear significant effect of the CMA-dependent secretome of PCs on the pro-inflammatory gene expression of endothelial cells (Fig. S5).

Administration of donor WT PCs after brain injury restores LAMP-2A expression and CMA activity in host PCs through their secretome

Our results thus far indicate that, in PCs, CMA activity promotes anti-inflammatory responses and seems to activate pathways involved in cell adhesion, communication, and stemness. All these pathways support a secretome which maintains stem cell properties in PCs. As PCs with multipotent stem cell properties are needed for tissue regeneration [15,23,24,131], we hypothesized that tissue inflammation would decrease CMA activity in PCs inducing an inflammatory phenotype with loss of stemness. This would produce a secretome unable to sustain pro-regenerative stem cell properties, negatively affecting tissue repair after injury. If this is true, then cellular therapy with CMA-efficient PCs should be able to decrease inflammation and promote tissue repair as it is expected to occur with MSCs [132,133]. We tested this hypothesis by intravenous administration of brain PCs in a lysolecithin-induced demyelinating mouse model [80] and using adipose tissue-derived MSCs (adMSCs) as a control treatment (Fig. 5A). We corroborated that exogenous PCs were able to access the brain tissue by showing that, three to eight days after administration, exogenous GFP-PCs appeared in the injured areas of the brain cortex and close to the hippocampus (Fig. 5A, Fig. S8A). They were

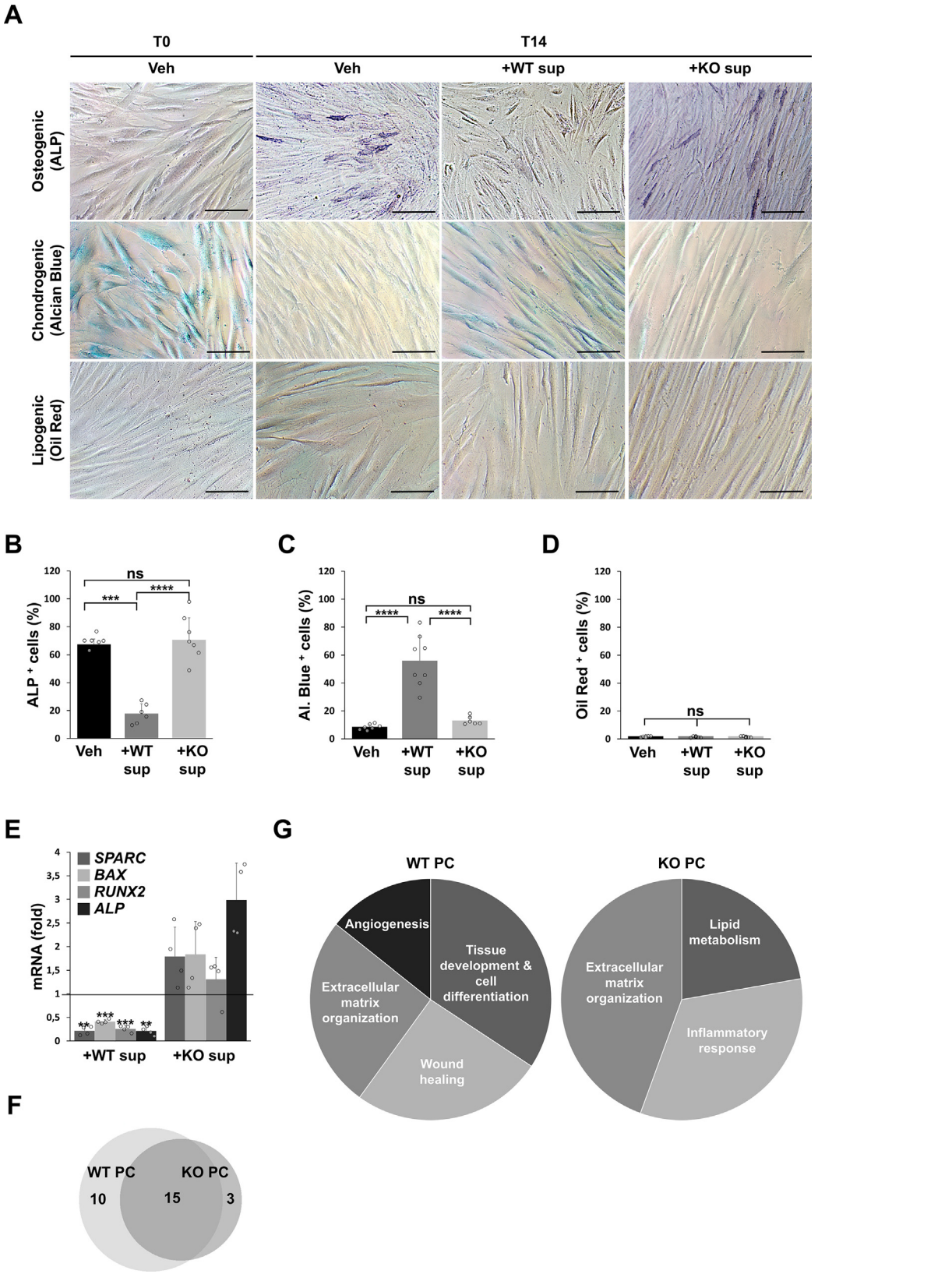
A
T0
T14
Veh
Veh
+WT sup
+KO sup
Osteogenic (ALP)
Chondrogenic (Alcian Blue)
Lipogenic (Oil Red)
B
ALP + cells (%)
ns
***
****
Veh
+WT sup
+KO sup
C
Al. Blue + cells (%)
ns
****
****
D
Oil Red + cells (%)
ns
E
SPARC
BAX
RUNX2
ALP
mRNA (fold)
+WT sup
+KO sup
F
WT PC
KO PC
10
15
3
G
WT PC
Angiogenesis
Tissue development & cell differentiation
Extracellular matrix organization
Wound healing
KO PC
Lipid metabolism
Extracellular matrix organization
Inflammatory response

Table 1
List of proteins exclusively identified in WT or KO PC secretome.

Accession	Protein name	GO Biological Process	Associated mechanisms	MW	WT PC Intensity	KO PC Intensity
P32261_MOUSE	Antithrombin-III	Wound healing Blood coagulation Hemostasis	Wound healingAngiogenesis	31,944	3,610,000	–
B1B0C7_MOUSE	Basement membrane-specific heparan sulfate proteoglycan core protein	Wound healing Cell differentiation Cell adhesion Vesicle-mediated transport Signaling Circulatory system development	Tissue development & cell differentiation Extracellular matrix and cytoskeleton organization Wound healingAngiogenesis	469,015	182,000	–
Q8BFZ3_MOUSE	Beta-actin-like protein 2	Cell motility Cytoskeleton organization	Extracellular matrix and cytoskeleton	42,004	5,990,000	–
P11087_MOUSE	Collagen alpha-1(I) chain	Extracellular matrix organization Cell differentiation Negative regulation of cell-substrate adhesion Signaling	Tissue development & cell differentiation Extracellular matrix and cytoskeleton organization Wound healingAngiogenesis	129,554	533,000	–
P01029_MOUSE	Complement C4-B	Inflammatory response Complement activation	Inflammatory response	192,912	1,300,000	–
E9PWX1_MOUSE	Dipeptidyl aminopeptidase-like protein 6	Regulation of potassium ion transmembrane transport Proteolysis	Inflammatory responseExtracellular matrix assembly	97,222	–	1,100,000
Q62356_MOUSE	Follistatin-related protein 1	Cell differentiation Cell motility Anatomical structure development	Tissue development & cell differentiationWound healing	34,553	1,050,000	–
E9Q1Z0_MOUSE	Keratin 90	Keratinization	Extracellular matrix assembly	58,223	–	229,000
P04104_MOUSE	Keratin, type II cytoskeletal 1	Keratinization Negative regulation of inflammatory response Intermediate filament organization	Tissue development & cell differentiationExtracellular matrix and cytoskeleton organization	65604,8	262,000	–
E9PUC2_MOUSE	Long-chain-fatty-acid–CoA ligase 3	Lipid metabolic process	Lipid metabolism	62,975	–	1,220,000
D3Z0P3_MOUSE	Serpin A11	Cell differentiation Negative regulation of endopeptidase activity Angiogenesis	Tissue development & cell differentiationAngiogenesis	26,200	262,000	–
A0A1L1SSH9_MOUSE	Osteonectin	Regulation of cell population proliferation Anatomical structure development Apoptosis Cell motility Pigmentation	Tissue development & cell differentiationWound healing	37,837	1,640,000	–
Q8VDF2_MOUSE	UHRF1 (ICBP90)-binding protein 1	Positive regulation of protein metabolic process Histone ubiquitination Cell cycle	Tissue development & cell differentiation	12,190	369,000	–

Fig. 3. CMA maintains a functional MSCs-like secretome in PCs. (**A**) Representative pictures show periodontal ligament stem cells (PDLSCs) that can spontaneously differentiate into an osteogenic lineage (T0). ALP, Alcian Blue, and Oil Red positive PDLSCs are shown after being incubated for 14 days (T14) with the control vehicle (veh), with supernatants from WT PCs (WT sup) or with supernatants from KO PCs (KO sup). Scale bar: 100 μm. (**B-D**) Graph represents the quantification of levels of positive cells for ALP activity (osteogenic lineage), alcian blue (chondrocytes), and Oil Red O (adipocytes) staining, respectively. All data represent mean ± SD obtained from at least five experiments represented as dots, independently; $^{***}p < 0.001$; $^{****}p < 0.0001$ (ANOVA with Tukey's post-test). (**E**) Quantification of the mRNA expression by qPCR of some genes involved in osteogenesis differentiation. Data show specifically the gene expression levels in PDLSCs (expressed as folds over control vehicle and normalized to *Actb* as the housekeeping reference gene expression) incubated with WT PCs sup or KO PCs sup. All data represent mean ± SD obtained from at least four experiments represented as dots, independently; $^{**}p < 0.001$; $^{***}p < 0.0001$ (ANOVA with Tukey's post-test). (**F**) Venn diagram of the secretome analysis of identified proteins in WT PCs and KO PCs. WT PCs secrete 10 exclusive proteins, sharing 15 proteins in common with KO PCs, which have 3 specific secreted proteins. (**G**) Chart shows the analysis of functional groups associated with pro-regenerative (left) and pro-inflammatory (right) mechanisms. These groups represent the percentage of proteins identified in both the secretome of WT PCs (right) and KO PCs (right) cultures from the total amount of identified proteins by mass spectrometry. The ratio between KO and WT PCs represents the most secreted proteins by each cell type. Twelve (34 %) of the proteins secreted by WT PCs were related to tissue development and cell differentiation functions (such as UHRF1 (ICBP90)-binding protein 1, follistatin-related protein 1, and SPARC), nine (26 %) were related to wound healing (such as plasminogen activator inhibitor 1 and perlecan), nine (26 %) to extracellular matrix organization (such as beta-actin-like protein 2) and five (17 %) to angiogenesis functions (such as antithrombin III). On the other hand, four (45 %) of the proteins secreted by KO PCs were related to extracellular matrix assembly (such as dipeptidyl aminopeptidase-like protein 6 and collagen alpha-1 chain), three (33 %) were related to inflammatory response (such as complement C3), and two (22 %) were related to lipid metabolism (such as long-chain-fatty-acid-CoA ligase 3). (For interpretation of the references to colour in this figure legend, the reader is referred to the web version of this article.)

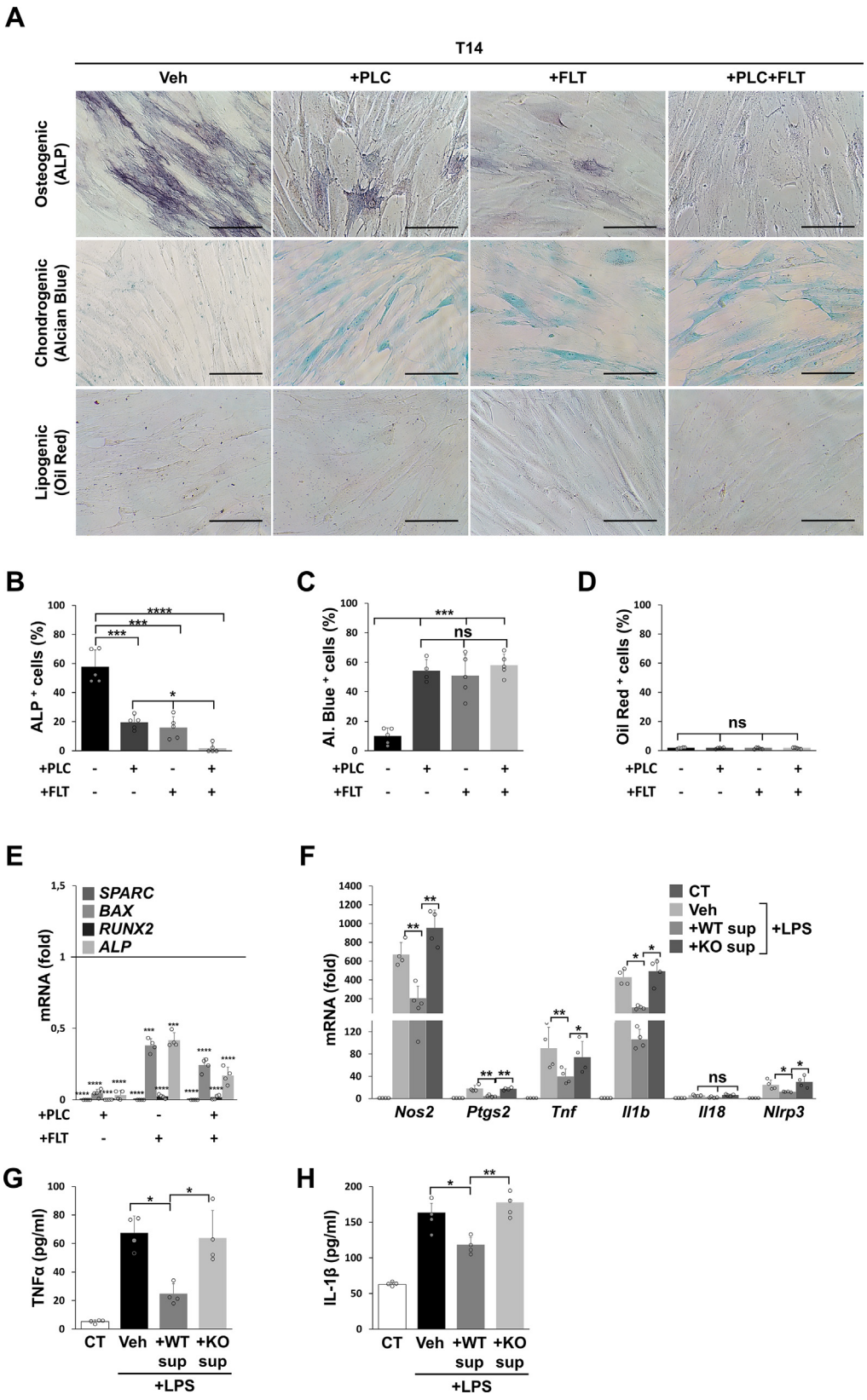
A
T14
Veh
+PLC
+FLT
+PLC+FLT
Osteogenic (ALP)
Chondrogenic (Alcian Blue)
Lipogenic (Oil Red)
B
ALP + cells (%)
C
Al. Blue + cells (%)
ns
D
Oil Red + cells (%)
ns
+PLC
+FLT
E
mRNA (fold)
SPARC
BAX
RUNX2
ALP
F
mRNA (fold)
CT
Veh
+WT sup
+KO sup
+LPS
Nos2
Ptgs2
Tnf
Il1b
Il18
Nlrp3
G
TNFα (pg/ml)
CT
Veh
+WT sup
+KO sup
+LPS
H
IL-1β (pg/ml)
CT
Veh
+WT sup
+KO sup
+LPS

hardly detected in later time points (Fig. S8B), as we previously described in the context of GB-conditioned PCs intracranially grafted or with intravenously injected exofucosylated GFP-PCs [21,63].

In our model, demyelination was assessed by quantifying loss of expression of the tissue regeneration marker myelin basic protein (MBP) after lysolecithin injection in the parietal cortex, between cerebral cortex and hippocampus, as it is an area of the brain where myelin is abundant [134]. Thus, MBP expression was reduced by a quarter in the white matter of the hippocampus (stratum lacunosum) and dentate gyrus (molecular layer) in the brains of injured mice (Fig. 5B, C). The lysolecithin diffusion in the tissue also produced cell death in the corpus callosum and the cerebral cortex (Fig. 5B, D). Furthermore, the tissue damage increased the cell expression of the neurotrophin BDNF in the injured areas (Fig. 5B, E). Importantly, the expression levels of MBP were significantly recovered, the cell death was reduced, and the BDNF-expressing cells disappeared in mice treated with donor brain PCs, as it occurred in those treated with the control treatment of adMSCs and compared to untreated mice or treated with the vehicle (Fig. 5B, C-E). Moreover, the treatment effect with brain PCs was clearly dependent on CMA, as CMA-deficient PC (KO PCs) administration lost the potential to promote tissue repair compared to the one with control PCs (WT PC) (Fig. 5). By opposite, KO PCs administration reduced by half the MBP expression (Fig. 5B, C) and doubled cell death compared to injured mice (Fig. 5B, D).

Our brain-injured mice model did not show any changes in the expression of the basement membrane marker of blood vessels, laminin [135–137], nor infiltration of CD3-positive cells, suggesting that the integrity of the BBB was not affected (Fig. S9). However, the demyelinating lesion increased nearly eight times the levels of inflammatory microglial cells, positive for the activation marker Iba-1, in the hippocampus of injured mice (Fig. 6A, B), probably to promote the elimination of myelin debris [81]. The appearance of cells in the damaged areas-surrounding brain thalamus expressing the cytokine IFNγ and the phagocytic cell marker CD68 were also increased five times in the brains of injured mice (Fig. 6A, C, D). Interestingly, KO PCs administration favored the entry of blood cells (Fig. 6A, D). Corroborating the tissue repair, all these pro-inflammatory markers were reduced after PC treatment, as it occurred with the control treatment with adMSCs (Fig. 6). Together, these results indicated that the administration of donor CMA-efficient PCs decreases inflammation and promotes tissue repair in the injured brain area in this animal model.

We next interrogated whether CMA in host PCs was affected in response to tissue injury in the brains of these animals. We used the expression of the following PC markers in the brain microvasculature: Alpha-smooth muscle actin (α-SMA), platelet-derived growth factor receptor-beta (PDGFR-β) or CD146 to identify PCs located in the microvessels of the damaged brain areas and quantified LAMP-2A expression levels as a marker of CMA activity (Fig. 7A, D). We found no differences in the total amount of PCs in the damaged areas of injured brains compared to control intact mice but importantly, LAMP-2A co-localizing with PC markers was significantly reduced by half (Fig. 7 and Fig. S10). These results indicate that CMA activity is downregulated in brain PCs during inflammation after a demyelinating injury. We then determined if CMA activity in PCs, responsible for maintaining MSC-like function, might contribute to tissue repair in this model of inflamed/injured tissue. We quantified LAMP-2A expression in host PCs after intravenous injection of donor brain tissue-derived PCs. LAMP-2A expression was restored in host PCs when mice were treated with donor CMA-efficient PCs (Fig. 7A-D), as it occurred in those treated with the adMSCs control treatment and compared to the untreated, intact controls and those treated with CMA-deficient PCs. Collectively, our findings suggest that intravenously administered donor PCs significantly restore CMA activity in host PCs, which is required to promote tissue regeneration, through ameliorating the brain inflammation by their CMA-dependent secretome.

Inflammatory signals reduce CMA activity and abrogate stemness gene expression in PCs

CMA activity is affected in other cell types and in different contexts of inflammation [49,138]. Thus, we wondered if inflammatory mediators released after brain injury could be responsible for the decrease of LAMP-2A and thus CMA activity observed in PCs in our *in vivo* inflammation model. First, we tested whether IFNγ, a cytokine produced by several cell types in the CNS during acute inflammation and associated with further tissue damage [139,140] was able to decrease LAMP-2A expression and therefore, the CMA activity in PCs, and we found that this was the case (Fig. 8A, B). We next analyzed how IFNγ alters the expression of some genes related to stemness and cell differentiation and found that IFNγ stimulation downregulated the expression of stemness genes and upregulated gene expression related to cell differentiation, including those involved in osteogenesis (Fig. 8C). Thus, IFNγ administration phenocopies the gene expression pattern in CMA-deficient PCs (Fig. 1A, C and Fig. 2D). Importantly, the restoring of LAMP-2A expression in PCs upon IFNγ stimulation (Fig. 8D) prevented the reduction of the stemness gene expression and thus, rescued their stemness phenotype (Fig. 8E). These results indicated that CMA modulation in response to the inflammatory mediator IFNγ affects MSC-like function of PCs.

Next, we evaluated if reduced CMA activity in PCs in response to inflammation was affecting their inflammatory properties by analyzing protein levels of the inflammatory mediators iNOS and COX-2 [49,141–143] in IFNγ-treated PCs. We found that CMA-deficient PCs showed a stronger proinflammatory phenotype independent of IFNγ stimulation (Fig. 8F, G). mRNA levels of both iNOS and COX-2 (*Nos2* and *Ptgs2*, respectively) were not affected by CMA deficiency (Fig. 8H). However, protein levels of COX-2 were increased four

Fig. 4. Stemness and anti-inflammatory properties of the CMA-dependent secretome of PCs. (**A**) Representative images of PDLSCs differentiation after incubation with proteins from WT PC supernatant (sup): perlecan (PLC, 5 μg/mL) and follistatin (FLT, 500 ng/mL), alone or combined, and vehicle (veh) for 14 days (T14). Scale bar: 100 μm. (**B-D**) Graphs represents the quantification of levels of positive cells for ALP activity, alcian blue, and Oil Red O staining, respectively. All data represent mean ± SD obtained from at least three experiments represented as dots, independently; $^{*}p < 0.05$; $^{***}p < 0.001$; $^{****}p < 0.0001$; ns indicates no statistical significance (ANOVA with Tukey's post-test). (**E**) Quantification of the mRNA expression by qPCR of some genes involved in osteogenesis differentiation. Data show specifically the gene expression levels (expressed as folds over control vehicle and normalized to *Actb* as the housekeeping reference gene expression) in PDLSCs incubated with PLC and FLT, alone or combined. All data represent mean ± SD obtained from at least three experiments represented as dots, independently; $^{***}p < 0.001$; $^{****}p < 0.0001$ (ANOVA with Tukey's post-test). (**F**) Quantification of the mRNA expression by qPCR of some genes involved in inflammatory responses in the microglial cell line BV2 (CT: control) activated with LPS (1 μg/mL) for 24 h (veh) and then incubated with WT PCs sup or KO PCs sup for 24 h after activation (expressed as folds over control non-activated and normalized to *Actb* and *Hrtp1* as housekeeping reference gene expression). Concentrated cultured media (veh) was used as control in activated cells. All data represent mean ± SD obtained from at least four experiments represented as dots, independently; $^{*}p < 0.05$; $^{**}p < 0.01$ (ANOVA with Tukey's post-test). (**G**) Levels of inflammatory cytokines TNF-α and (**H**) IL-1β secreted by unstimulated microglial cells (CT) or activated with LPS (1 μg/mL) for 24 h (veh) and incubated with WT PCs sup or KO PCs sup for 48 h after stimulation. Concentrated cultured media (veh) was used as control in activated cells. All data represent mean ± SD obtained from at least four experiments represented as dots, independently; $^{*}p < 0.05$; $^{**}p < 0.01$ (ANOVA with Tukey's post-test). (For interpretation of the references to colour in this figure legend, the reader is referred to the web version of this article.)

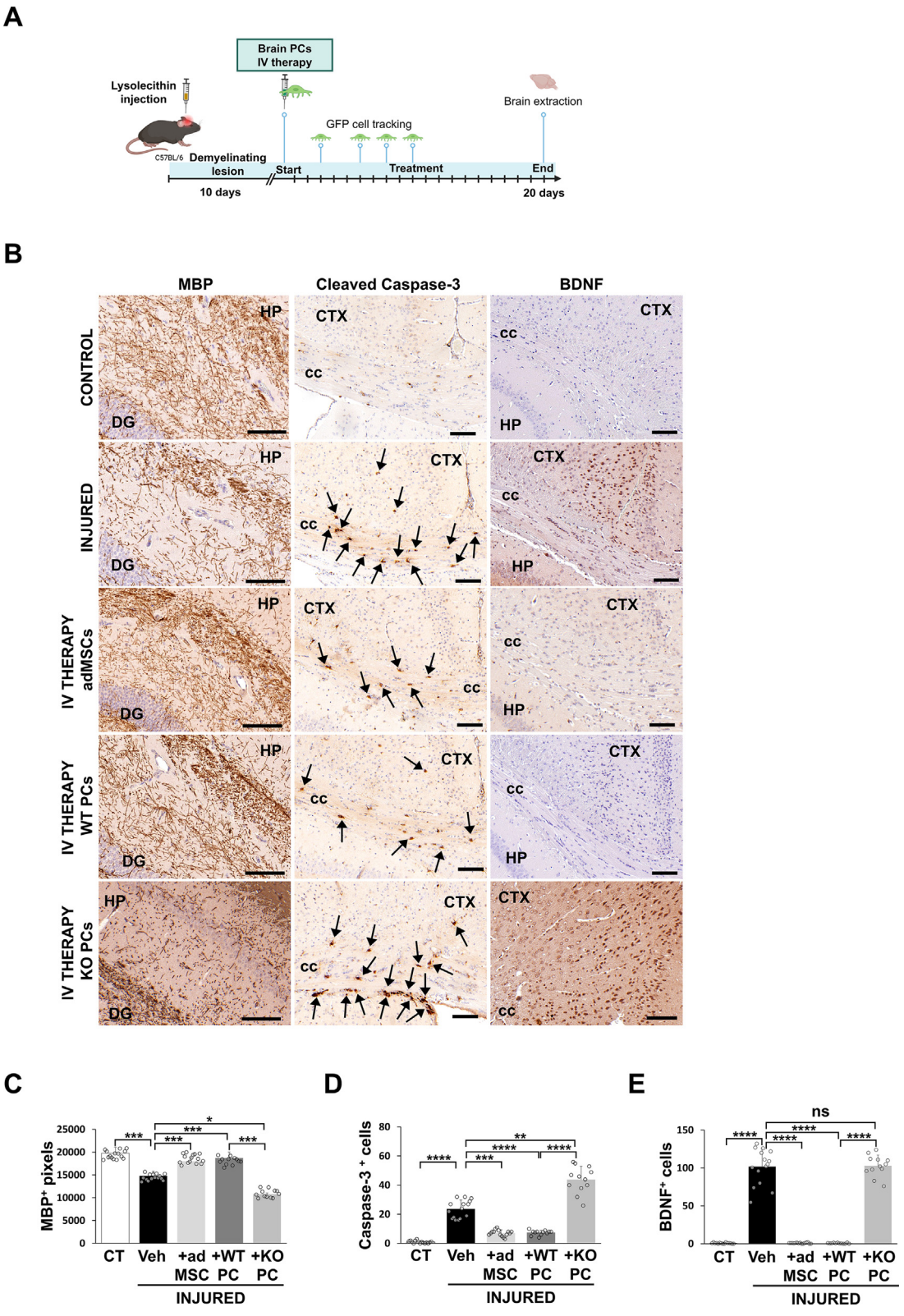
A
Brain PCs IV therapy
Lysolecithin injection
C57BL/6
Demyelinating lesion
10 days
Start
GFP cell tracking
Treatment
Brain extraction
End
20 days
B
MBP
Cleaved Caspase-3
BDNF
CONTROL
INJURED
IV THERAPY adMSCs
IV THERAPY WT PCs
IV THERAPY KO PCs
HP
DG
CTX
cc
C
MBP+ pixels
D
Caspase-3+ cells
E
BDNF+ cells
ns
CT
Veh
+ad MSC
+WT PC
+KO PC
INJURED

times in KO PCs (Fig. 8G), indicating that COX-2 protein levels are regulated by CMA in PCs, while iNOS is not (Fig. 8G and H). IFNγ upregulated more than ten times the iNOS gene expression in both WT and CMA-deficient PCs compared to basal levels, while it did not change the expression of COX-2 gene (Fig. 8H). Then, increased iNOS expression at protein levels was caused by IFNγ-mediated increased transcription. In contrast, IFNγ increased COX-2 protein levels only in WT PCs, indicating that this accumulation was due to IFNγ-mediated downregulation of CMA activity (Fig. 8G). These results suggest that intrinsic CMA activity modulates the proinflammatory phenotype of the PC by degrading or preventing accumulation of positive regulators of inflammation such as COX-2, which might contribute to inflammation in the injured brain (Fig. 4F-H, Fig. 6A-D, and Fig. S7). We did not observe differences in macroautophagic activity between WT and KO PCs (Fig. S11), supporting that the observed phenotype is primarily a consequence of CMA deficiency. Our results support that CMA contributes to the remodeling of the proteome of PCs under conditions of homeostasis, enhancing a proinflammatory phenotype in response to IFNγ stimulation by downregulating CMA activity.

Overall, these findings highlight CMA activity in PCs as a key protective mechanism by maintaining PC stemness and modulating cell homeostasis to prevent hyperinflammation and promote tissue regeneration (Fig. 9).

Discussion

PCs exhibit some properties of MSCs and contribute to tissue repair after injury in different pathologies [23,24]. In addition, these cells are capable of differentiating into other cell types by a mechanism that is not well understood yet [25–27]. We have previously reported that GB induces an aberrant upregulation of CMA in PCs that modulates their immune function and some MSC-like properties to support tumor growth [21]. GB-induced CMA in the brain PCs alters some of these properties, including increased secretion of regenerative, angiogenic, and anti-inflammatory factors [21,62,63]. Thus, we have previously found that intrinsic CMA in PCs should explain some of their pro-tumor biology and support the potential of CMA-deficient PCs to be used as antitumor therapeutical tools [21,62,63]. Based on the cellular processes differentially modulated by CMA in the host PC, these cells might also be therapeutically effective targets in the context of other diseases by enhancing their MSC-like function.

Here, we provide new data supporting our hypothesis, showing that CMA-deficient PCs lose their functional resemblance with MSCs and acquire a differentiated phenotype (Figs. 1 and 2). CMA-defective PCs predominantly show a differentiation phenotype towards the lipogenic lineage (Fig. 1C, Fig. 2A, B, C, and Fig. S3), and this differentiation is spontaneously switched to a different lineage during long-term culture without any conditioned media for specific cell lineage differentiation (Fig. 2A, B, C). Even though we did not check for a later osteogenic differentiation phenotype, it is important to mention that other authors have observed calcium deposits in PCs from different tissues [144–146] using inductor media of osteogenic differentiation to promote bone tissue regeneration [144,145,147,148]. Brain pericytes may probably also present this phenotype, but we only evaluated their spontaneous multipotency to verify the changes that CMA deficiency was causing in their mesenchymal properties.

In contrast, PCs presenting functional CMA remain undifferentiated and maintain their capacity to differentiate into either osteogenic, adipogenic, or chondrogenic cell lineages. Recent results in other biological systems have demonstrated the relevance of autophagy for maintaining the stemness condition of HSC, whereas the ubiquitin-dependent proteasome pathway is used for differentiating HSPCs [149]. This supports the idea that CMA degrades proteins that regulate cell differentiation in PCs when they are growing *ex vivo* immediately after isolation or even after several days in culture, maintaining PC multipotency as MSCs.

Although our results indicate that CMA-defective PCs can be spontaneously differentiated into cells with an osteogenic phenotype in culture (Fig. 2A, B, D), basal levels of CMA prevent lipogenic cell differentiation in resting conditions (Fig. 1C and Fig. 2A, B, C and Fig. S3). In line with the results, PCs have/acquire some properties [15,23,144,145,147,150] but not others of MSC [4,5,21,65,151]. Thus, brain PCs may not present capabilities to specifically differentiate to adipose cell lineage, as particularly those MSCs derived from dental pulp or periodontal ligament, with also neural crest origin and a tendency to differentiate into osteogenic and none-adipose tissue [102,112,152]. The results show that osteogenic gene expression is not induced in CMA-defective PCs in resting conditions, but CMA activity in basal levels seems to control genes involved in cell differentiation to regulate their osteogenic lineage (Fig. 2C). Moreover, PCs with reduced CMA activity in response to inflammation lead to the induction of osteogenic gene expression with a clear loss of stemness. This finding supports that cell differentiation in PCs is prevented through CMA activity to maintain their MSC-like function including inflammatory properties (Fig. 1C, 4F-H, and 8D-H). The results showing that CMA-defective PCs present a prone lipogenic lineage with upregulated lipogenic and inflammatory genes such as *Fabp4*, *Pparg*, *Ptgs1*, *Cebpa and Plin1-4* (Fig. 1C and Fig. 2C), suggest a predifferentiated cell type prone to the adipogenic cell lineage. This is due to the failure in degrading proteins involved in the lipidic metabolism and the control of cell differentiation from one lineage to another [58,153,154]. Conversely, this phenotype does not contribute to protect from inflammation and seems to release adipokines via altered CMA activity contributing to inflammation [49,63,129,138,155,156].

Interestingly, our characterization of CMA-deficient PCs indicates that in the absence of CMA activity, PCs are entailed to type II PCs which differentially to adipogenic type I that can produce fibrosis [157,158]. They are nestin-positive cells that can partici-

Fig. 5. Intravenous PC administration promotes tissue repair in lesioned brains. (**A**) Timeline of demyelinating lesion and treatment with PCs. Mice were treated intravenously with brain PCs or adMSCs, ten days post-lesion. Brain GFP-PCs were used as tracking cells. After three weeks (twenty days), mice were euthanized, and brains were extracted. (**B**) Expression of the regenerative marker myelin basic protein (MBP), the cleaved caspase-3 as cell death marker (positive cells marked with arrows), and the brain-derived neurotrophic factor (BDNF) in brain tissue lesioned with lysolecithin and after treatment with brain donor PCs. Images are representative of control mice (CT) and injured mice untreated (Veh) or treated with control adMSCs, WT or KO PCs. Representative images of MBP expression show the hippocampus (HP) and dentate gyrus (DG) areas where the lysolecithin was injected. Caspase-3 and BDNF images show the injured areas by lysolecithin diffusion in the corpus callosum (cc) and cerebral cortex (CTX). Scale bars: 100 μm. (**C**) Quantification of MBP expression relative to total injured area of MBP immune-positive particles (pixels) per brain in, at least, four fields. All data represent mean ± SD obtained from at least three experiments represented as dots, independently; $^{***}p < 0.001$; ns indicates no statistical significance (ANOVA with Tukey's post-test). (**D**) Quantification of caspase-3 immune-positive cells per brain in at least, four fields. All data represent mean ± SD obtained from at least, three experiments represented as dots, independently; $^{**}p < 0.01$; $^{***}p < 0.001$; $^{****}p < 0.0001$ (ANOVA with Tukey's post-test). (**E**) Quantification of BDNF immune-positive cells in, at least, four fields per brain. All data represent mean ± SD obtained from at least three experiments represented as dots, independently; $^{*}p < 0.05$; $^{**}p < 0.01$; $^{***}p < 0.001$ (ANOVA with Tukey's post-test).

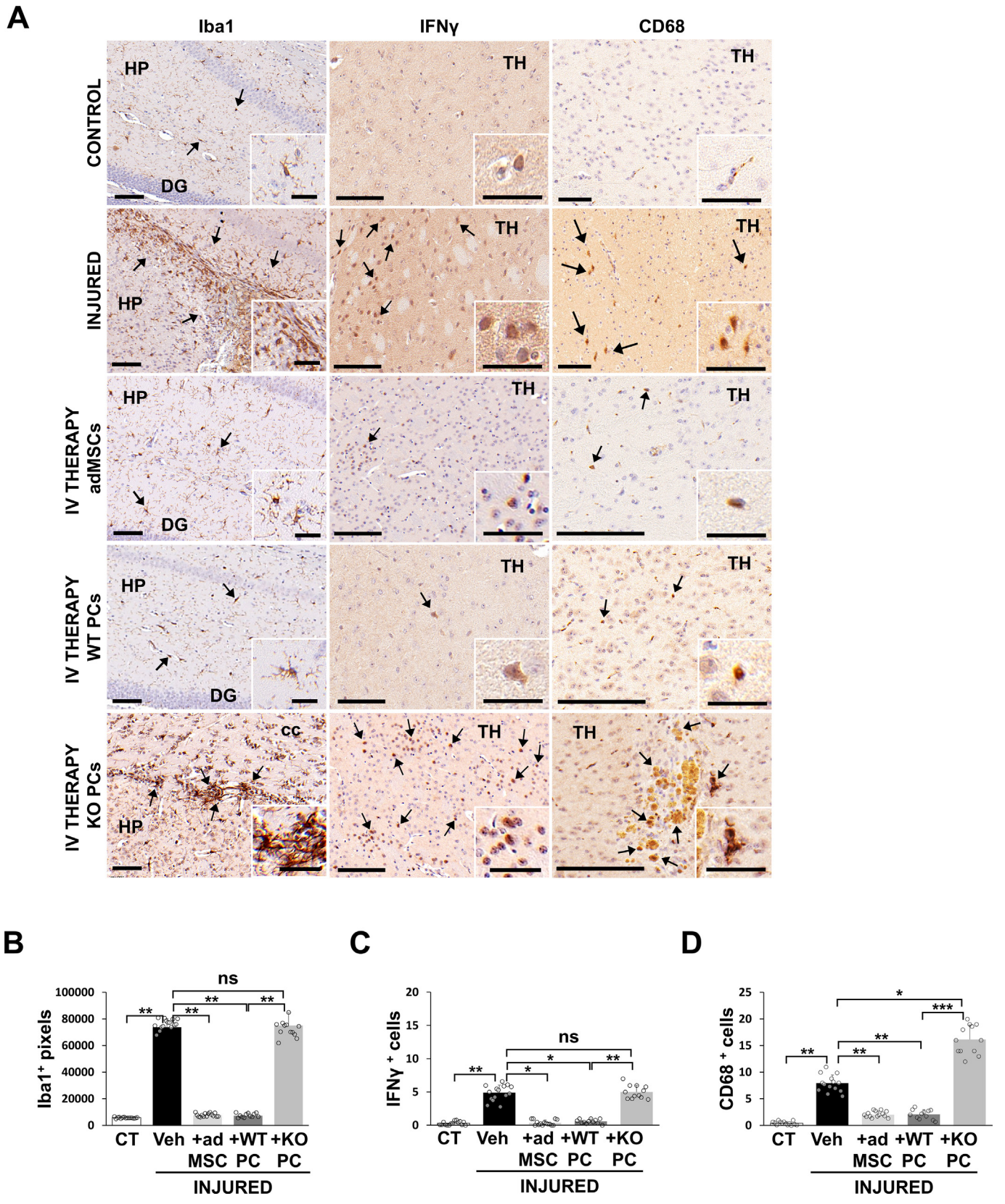

Fig. 6. Intravenous PC administration decreases inflammation in lesioned brains. (**A**) Expression of the inflammation markers Iba-1, IFN$_\gamma$, and the activation phagocytic marker CD68 (positive cells marked with arrows) in the hippocampus (HP) and the thalamus (TH) close to the brain area lesioned with lysolecithin and after treatment with donor brain PCs. Images are representative of control mice (CT) and injured mice untreated (Veh) or treated with control adMSCs, WT or KO PCs. Scale bars: 100 μm. Bottom right corner panels show Iba-1, IFN$_\gamma$, and CD68 positive cells in bigger magnification. (**B-D**) Relative quantification of Iba-1 positive particles (pixels) or IFN$_\gamma$, and CD68 positive cells around the injured area per brain in at least, four fields. All data represent mean ± SD obtained from at least, three experiments represented as dots, independently; $^{**}p < 0.01$; $^{***}p < 0.001$; ns indicates no significance (ANOVA with Tukey's post-test).

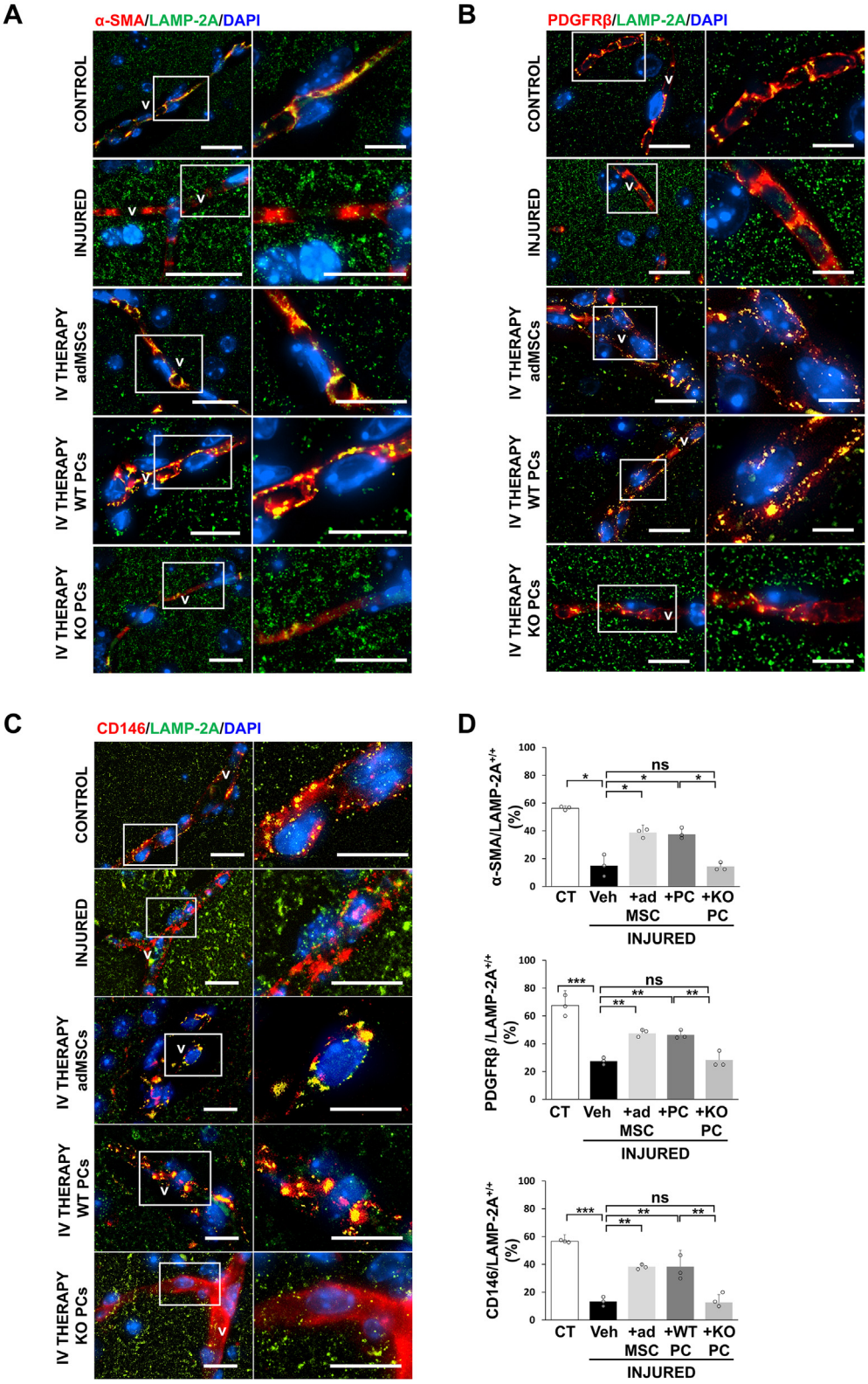

Fig. 7. Donor PC therapy restores CMA in host PCs in damaged tissue. **(A)** Representative images showing co-localization of puncta pattern expression of LAMP-2A protein (green) with a PC marker, α-SMA (red), analyzed in host PCs of microvessels (v) of control mice, in mice brain with lesioned areas (injured) and treated intravenously with control adMSCs and with donor brain WT or KO PCs. Nuclei were stained with DAPI (blue). Scale bar: 100 μm. Right panels show bigger magnification of double positive cells. (**B**) Representative images showing co-localization of puncta pattern expression of LAMP-2A protein (in green) with a PC marker, PDGFRβ (in red), analyzed in host PCs of microvessels (v) of control mice, in mice brain with lesioned areas and treated intravenously with control adMSCs and with donor brain WT or KO PCs. Right panels show bigger magnification of double positive cells. Nuclei were stained with DAPI (blue). Scale bars: 100 μm. **(C)** Representative images showing co-localization of puncta pattern expression of LAMP-2A protein (in green) with a PC marker, CD146 (in red), analyzed in host PCs of microvessels (v) of control mice, in mice brain with lesioned areas and treated intravenously with donor brain PC. Right panels show bigger magnification of double positive cells (Scale bars: 20 μm). Nuclei were stained with DAPI (blue). Scale bars: 100 μm. (**D**) Relative quantification of percentage of PCs in brain microvessels expressing the PC marker α -SMA (n = 40 α -SMA$^+$ PCs per condition), PDGFRβ (n = 20 PDGFRβ$^+$ PCs per condition), or CD146 (n = 35 CD146$^+$ PCs per condition) and the CMA receptor LAMP-2A (PC/LAMP-2A$^{+/+}$) over total PCs. All data represent mean ± SD obtained from at least, three experiments represented as dots, independently; $^*p < 0.05$; $^{**}p < 0.01$; $^{***}p < 0.001$; ns indicates no statistical significance (ANOVA with Tukey's post-test). (For interpretation of the references to colour in this figure legend, the reader is referred to the web version of this article.)

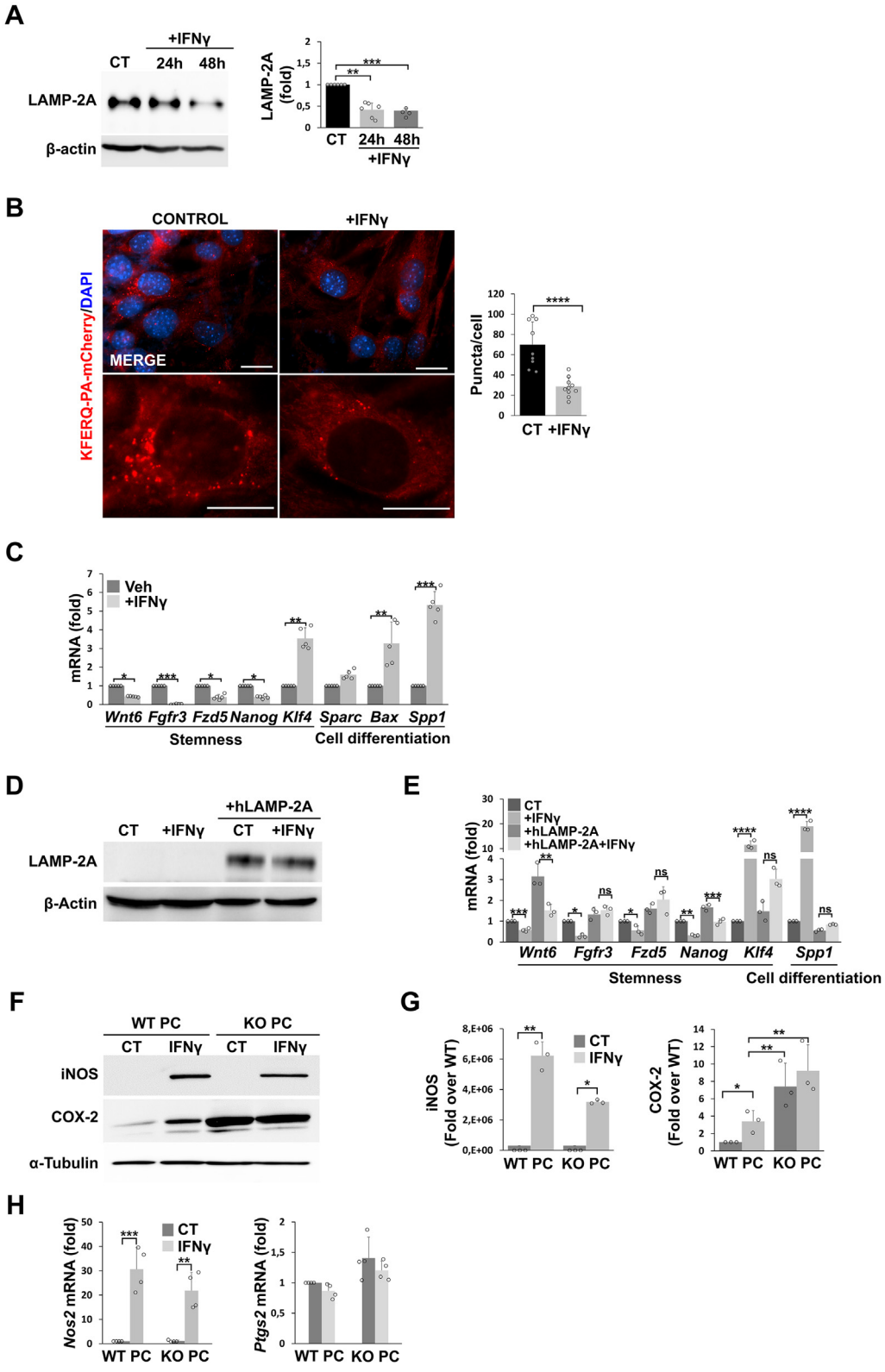
A
+IFNγ
CT
24h
48h
LAMP-2A
β-actin
LAMP-2A (fold)
CT
24h
48h
+IFNγ
B
CONTROL
+IFNγ
KFERQ-PA-mCherry/DAPI
MERGE
Puncta/cell
CT +IFNγ
C
Veh
+IFNγ
mRNA (fold)
Wnt6 Fgfr3 Fzd5 Nanog Klf4 Sparc Bax Spp1
Stemness
Cell differentiation
D
+hLAMP-2A
CT
+IFNγ
CT
+IFNγ
LAMP-2A
β-Actin
E
CT
+IFNγ
+hLAMP-2A
+hLAMP-2A+IFNγ
mRNA (fold)
Wnt6
Fgfr3
Fzd5
Nanog
Klf4
Spp1
Stemness
Cell differentiation
F
WT PC
KO PC
CT
IFNγ
CT
IFNγ
iNOS
COX-2
α-Tubulin
G
CT
IFNγ
iNOS (Fold over WT)
COX-2 (Fold over WT)
WT PC
KO PC
H
CT
IFNγ
Nos2 mRNA (fold)
Ptgs2 mRNA (fold)
WT PC
KO PC

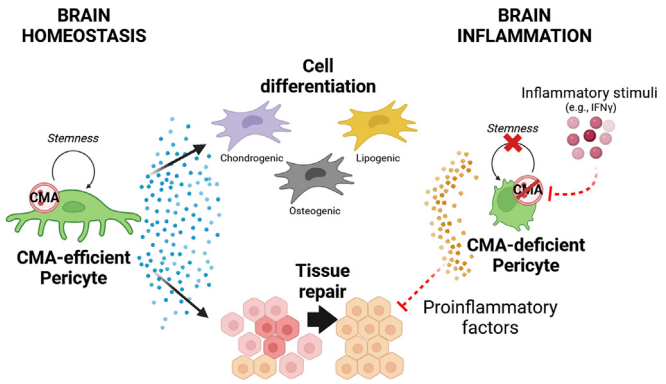

Fig. 9. CMA role and modulation in PCs of brain homeostasis and during inflammation. During brain homeostasis (left), intrinsic CMA in PCs maintains their stemness MSC-like properties such as proliferation, adhesion, and potential to differentiate into different cell lineages. CMA is then required to maintain the MSC-like-function of PCs as mural cells in the brain through their secretome, sustaining the secretion of pro-regenerative and immunomodulatory factors that can maintain the stemness of surrounding PCs and ameliorates inflammation, therefore, controlling their cell differentiation and contributing to tissue repair. In lesions or injuries that cause brain inflammation (right), proinflammatory cytokines such as IFNγ modulate the MSC-like properties of PCs through CMA, altering its stemness gene expression pattern and the regenerative properties of their secretome. Thus, they lose their pluripotency, alter their secretome composition becoming non-functional, and trigger an inflammatory phenotype containing proinflammatory factors that prevent tissue repair.

pate in normal and tumoral angiogenesis, and present regenerative properties in skeletal muscle (Fig. S4) [25,26]. However, PCs with defective CMA show altered size and proliferation rate (Fig. S5A, B), which may be explained as a consequence of CMA-dependent DEGS related to cell adhesion properties (Fig. 1A), affecting PC adhesion required for vascular stabilization during tissue regeneration [99,158]. Furthermore, accumulation of HIF-1α, a substrate degraded by CMA, might modify PC metabolism affecting some MSCs-like properties in CMA-defective PCs (Fig. S5A) [12,97,98]. These results suggest that decreased CMA activity promotes a pre-differentiated PC stage through the accumulation of specific negative regulators and in combination with the downregulation of EMT markers, preventing PC stemness (Fig. S5B). In addition, our data suggests that CMA activity might be also necessary to improve tissue homing as we identified downregulated DEGs in CMA-deficient PCs related to cell adhesion and communication pathways (Fig. 1A, right) and loss of adhesion cell markers (Fig. S5B).Our data show that all these changes in CMA-defective PCs lead to a PC which lacks functional MSC-like properties. The PC secretome does not affect *in vitro* cell differentiation of MSCs, a process that might contribute to tissue repair after injury. Conversely, PCs with basal levels of effective CMA activity show a secretome that prevents cell differentiation and maintains the stemness in MSCs needed for tissue repair (Fig. 3). Loss of PC multipotent properties directly impacts the PC secretome (Fig. 3) which affects neighboring cells (Fig. 4). The identification of CMA-dependent secreted proteins in PCs, including proteins implicated in reducing inflammation [107,124] and tissue repair and regenerative processes (Fig. 3F, G and Table S1), corroborates our previous results for stemness maintenance. Importantly, the dysfunctional secretome of CMA-deficient PCs and the identification of the secreted proteins, dipeptidyl aminopeptidase-like protein 6 and long-chain-fatty-acid-CoA ligase (Fig. 3F and Table 1) [125,128,129] suggest that CMA is needed to modulate the PC proteome required for its lipidic metabolism and efficient interactions with the extracellular matrix. Thus, an altered proteome implicated in lipidic metabolism and PC-extracellular matrix interactions, because of deficient intrinsic CMA levels, might contribute to a PC inflammatory phenotype [49,58,63] and a defective size and cell interactions through inefficient filopodia, key for cell communication and migration [126,127]. This result also explains how the functional secretome dependent on CMA of donor PCs can contribute, at least in part, to tissue repair and regeneration in response to acute inflammation (Figs. 4-6). Importantly, our results *in vitro* were corroborated *in vivo* in response to inflammation in a demyelinating mouse model. Inflammation in the brain was decreased after intravenous administration of PCs with efficient CMA (Fig. 6 and Fig. S8). We found that the function of the PC in this mouse model was regulated by CMA activity, specifically mediated by a decrease in LAMP-2A expression during inflammation, which in turn downregulates CMA activity. Importantly, LAMP-2A expression, and thus CMA activity, was restored after treatment with donor CMA-efficient PCs, whereas CMA-deficient PCs did not have this effect (Fig. 7). Consequently, tissue repair and reduced inflammation in the damaged tissue microenvironment impair the inflammatory signals (Figs. 5 and 6) that affect the CMA activity levels in host PC (Fig. 7) and thus, promote a restored MSC-like phenotype (Figs. 1, 5 and 8), contributing to prevent inflammation through regulation of proinflammatory factors (Fig. 1A, Fig. 6 and Fig. 8).

Although other authors showed that CMA can be modulated by different inflammatory stimuli in several pathological contexts and cell types [49,54,138], this is the first time that CMA activity is shown to be modulated by the proinflammatory cytokine IFNγ.

Fig. 8. Reduced CMA activity in response to IFNγ downregulates the stemness gene expression in PCs. (**A**) Expression levels of LAMP-2A protein in IFNγ-treated PCs (20 ng/mL) for 24 and 48 h and compared to controls. All data represent mean ± SD obtained from at least three experiments represented as dots, independently; $^{**}p < 0.01$; $^{***}p < 0.001$ (Student's *t*-test). (**B**) CMA activity was measured by the number of puncta relative to CMA substrates at the lysosomal membrane and expressed by the KFERQ-PA-mCherry reporter in IFNγ-treated PCs for 24 h compared to basal activity in control PCs. Nuclei were stained with DAPI (blue). All data represent mean ± SD obtained from at least, three experiments represented as dots, independently. $^{****}p < 0.0001$ (Student's *t*-test). Scale bar: 50 μm. (**C**) Quantification of the mRNA expression by qPCR, of some downregulated genes that were identified in the downregulated pathways related to stemness from CMA-dependent DEGs and some upregulated genes related to osteogenic cell differentiation. Data show specifically the gene expression levels in IFNγ-treated PCs for 24 h (relative to PC basal levels) and expressed as folds over untreated (control) and normalized to *Actb* and *Hrtp1* as housekeeping reference gene expression. *Klf4* gene was used as an inflammatory response control. All data represent mean ± SD obtained from at least, five experiments represented as dots, independently; $^{*}p < 0.05$; $^{**}p < 0.01$; $^{***}p < 0.001$; $^{****}p < 0.0001$ (Student's *t*-test). (**D**) Expression levels of LAMP-2A protein in PCs transfected with human LAMP-2A or mCherry backbone plasmids and incubated or not with IFNγ (20 ng/mL) for 24 h. All data represent mean ± SD obtained from at least six experiments represented as dots, independently. (**E**) Quantification of the mRNA expression by qPCR of some genes related to stemness in PCs transfected with human LAMP-2A or mCherry backbone plasmid and incubated or not with IFNγ (20 ng/mL) for 48 h, expressed as folds over untreated (Control) and normalized to *Actb* and *Hrtp1* as housekeeping reference gene expression. *Klf4* gene was used as an inflammatory response control. All data represent mean ± SD obtained from at least, five experiments represented as dots, independently; $^{*}p < 0.05$; $^{**}p < 0.01$; $^{***}p < 0.001$; $^{****}p < 0.0001$; ns indicates no significance (ANOVA with Tukey's post-test). (**F**) Expression levels of the inflammatory mediators iNOS and COX-2 in WT PCs and KO PCs treated or not (control) with IFNγ for 24 h. (**G**) Densitometric quantification of iNOS and COX-2 protein levels expressed as folds over WT levels. (**H**) Quantification of the mRNA expression by qPCR of iNOS (*Nos2*) and COX-2 (*Ptgs2*) treated for 20 h with IFNγ expressed as folds over untreated (Control) and normalized to *Actb* and *Hrtp1* as housekeeping reference gene expression. All data represent mean ± SD obtained from at least, four experiments represented as dots, independently; $^{*}p < 0.05$; $^{**}p < 0.01$; $^{***}p < 0.001$ (ANOVA with Tukey's post-test). (For interpretation of the references to colour in this figure legend, the reader is referred to the web version of this article.)

In the context of brain inflammation, other studies have shown that CMA is affected during aging or inflammation [47,54,159] and can be modulated improving its activity with several modulators [33,34,48,55]. In this work, we identify that CMA activity can be affected, specifically in PCs, in response to IFNγ, and presumably, by others inflammatory cytokines in the context of tissue inflammation (Figs. 4 and 5), and it can be modulated by the MSCs-like secretome of PCs improving its activity. Thus, our findings support previous studies indicating that CMA is essential for brain homeostasis and show that it is essential in PCs to contribute to brain tissue repair.

Our results are specific to mammalian inflammation as the presence of LAMP-2A, the limiting factor of CMA, and its regulatory mechanisms (e.g., cytokines produced during brain inflammation) are limited to mammals. However, similar mechanisms of protein degradation have been recently found in fish and birds [160–163]. Thus, the study of this lysosomal catabolic pathway might be explored in other species as new models of study for identifying new roles or functions. Another caveat in this study is the technical limitation to distinguish PC and MSC populations because they are very heterogeneous populations without specific biomarkers to differentiate from each other. However, a PC secretome with pluripotent properties and MSC-like function dependent on CMA supports strongly that PCs act as MSCs in the brain (Figs. 2-4), allowing to hypothesize that CMA might be required in PCs not only to modulate their own stem cell behavior but also to impact the properties of other brain stem cells (Fig. 4F-H and S7), facilitating tissue regeneration. Intrinsic CMA activity in PCs might also be needed to protect the brain from inflammation resulting from the tissue damage itself (Fig. 6A-D and 7) and thus, to contribute to tissue repair. Overall, our results suggest that inflammation-mediated decrease of CMA activity in host PCs after brain injury (Figs. 7 and 8) affect cell homeostasis in brain blood microvessels through the loss of their MSC-like properties, exacerbating inflammation and altering stem cell activity through their dysfunctional secretome (Fig. 9). Conversely, the maintenance of an effective CMA activity in PCs makes them a potential source of therapeutic cell products to ameliorate pathogenesis in the context of diseases associated with regeneration of inflamed tissue by manipulating PC CMA activity and in turn their secretome.

Conclusion

Our results suggest that inflammation-mediated reduced CMA activity in host PCs, after brain injury, disrupts microvessel homeostasis, worsens inflammation, and impairs stem cell properties via a dysfunctional secretome. The CMA maintenance or improvement in PCs could support tissue regeneration by modulating their secretome, offering therapeutic potential for brain inflammation and likely other pathologies, where PCs play a pivotal role in response to inflammatory signals.

Author Contributions

MDS performed the most part of the experiments; RV designed and performed some experiments; CMM, MDS, and RV analyzed and interpreted data. DG-B, SM, and RV contributed to the animal model induction and PC therapy. FJR provided help in the qualitative analysis of the secretome and the data interpretation on inflammation. MM-M contributed with technical support. JR-M and FP provided advice on gene analysis related to MSCs. DG-B, FJR, AGZ, and SM were involved in data discussion. JMM and FJR contributed new reagents/analytic tools. MDS and RV wrote the manuscript. FJR and AGZ edited the manuscript. RV conceived, designed, and coordinated the study.

Ethics Statement

All animal procedures were approved and performed according to the guidelines set by the Institutional Animal Care and Use Committee of the University of Murcia, Spain (approved protocol A13150201) and of the Institute of Biomedical Research of Murcia (IMIB) Pascual Parrilla, Spain (approved protocol A13210202).

Data availability

The original contributions presented in the study are publicly available in ENA under accession number PRJEB48545.

Declaration of competing interest

The authors declare that they have no known competing financial interests or personal relationships that could have appeared to influence the work reported in this paper.

Acknowledgments

This work was mainly developed by Seneca 20840/PI/18 funded by Seneca Foundation ‘‘Agencia de Ciencia y Tecnología de la Región de Murcia”, by Ramon y Cajal (RYC) 2019-027520-I funded by Ministerio de Ciencia, Innovación y Universidades (MCIU) and Agencia Estatal de Investigación (AEI) MCIU/AEI/10.13039/50110-0011033, as ‘‘ European Social Fund (ESF) Investing in your future”, and by PID2020-114010RB-I00 and PID2023-149111OB-I00 funded by MICIU/AEI/10.13039/50110001 1033 and Fondo Europeo de Desarrollo Regional (FEDER), UE (to RV). It was also partially supported by CaixaImpulse CI23-20487 funded by ¨La Caixa¨ Foundation (to RV) and by Spanish Network of Advanced Therapies (TERAV), RICORS subprogram (to AGZ, FP, SM and JMM), funded by Instituto de Salud Carlos III and co-funded by European Regional Development Fund (ERDF)-Next Generation EU ‘‘Plan de Recuperación, Transformación y Resiliencia”. FJR was supported by fellowship RYC2019-571 027799-I funded by MCIU/AEI.

We thank Jose Luis Ferran at Human Anatomy Deaprtment, UMU and Pablo Pelegrín’s lab at Experimental Surgery Unit, IMIB for his always kind help providing tools for this study. We thank Professor Ana Maria Cuervo at the Developmental Molecular Biology Department and Professor Fernando Macian at the Pathology Department of Albert Einstein College of Medicine (New York, United States) for all their kind help providing the deficient CMA mice and the CMA reporter and in the initial design of this study and data discussion. We thank the Pathology, Bioinformatic and Animal facilities of IMIB.

Appendix A. Supplementary data

Supplementary data to this article can be found online at https://doi.org/10.1016/j.jare.2025.04.015.

References

[1] Daneman R, Zhou L, Kebede AA, Barres BA. Pericytes are required for blood–brain barrier integrity during embryogenesis. Nature 2010;468:562–6. doi: https://doi.org/10.1038/nature09513.

[2] Sweeney MD, Ayyadurai S, Zlokovic BV. Pericytes of the neurovascular unit: key functions and signaling pathways. Nat Neurosci 2016;19:771–83. doi: https://doi.org/10.1038/nn.4288.

[3] Brown LS, Foster CG, Courtney J-M, King NE, Howells DW, Sutherland BA. Pericytes and neurovascular function in the healthy and diseased brain. Front Cell Neurosci 2019;13:00282. doi: https://doi.org/10.3389/fncel.2019.00282.
[4] Török O, Schreiner B, Schaffenrath J, Tsai H-C, Maheshwari U, Stifter SA, et al. Pericytes regulate vascular immune homeostasis in the CNS. Proc Natl Acad Sci 2021;118:e2016587118. doi: https://doi.org/10.1073/pnas.2016587118.
[5] Rustenhoven J, Jansson D, Smyth LC, Dragunow M. Brain pericytes as mediators of neuroinflammation. Trends Pharmacol Sci 2017;38:291–304. doi: https://doi.org/10.1016/j.tips.2016.12.001.
[6] Duan L, Zhang X-D, Miao W-Y, Sun Y-J, Xiong G, Wu Q, et al. PDGFRβ cells rapidly relay inflammatory signal from the circulatory system to neurons via chemokine CCL2. Neuron 2018;100:183–200.e8. doi: https://doi.org/10.1016/j.neuron.2018.08.030.
[7] Matsumoto J, Dohgu S, Takata F, Machida T, Bölükbaşi Hatip FF, Hatip-Al-Khatib I, et al. TNF-α-sensitive brain pericytes activate microglia by releasing IL-6 through cooperation between IκB-NFκB and JAK-STAT3 pathways. Brain Res 2018;1692:34–44. doi: https://doi.org/10.1016/j.brainres.2018.04.023.
[8] Smyth LCD, Rustenhoven J, Park T-I-H, Schweder P, Jansson D, Heppner PA, et al. Unique and shared inflammatory profiles of human brain endothelia and pericytes. J Neuroinflammation 2018;15:138. doi: https://doi.org/10.1186/s12974-018-1167-8.
[9] Jansson D, Scotter EL, Rustenhoven J, Coppieters N, Smyth LCD, Oldfield RL, et al. Interferon-γ blocks signalling through PDGFRβ in human brain pericytes. J Neuroinflammation 2016;13:249. doi: https://doi.org/10.1186/s12974-016-0722-4.
[10] Nortley R, Korte N, Izquierdo P, Hirunpattarasilp C, Mishra A, Jaunmuktane Z, et al. Amyloid β oligomers constrict human capillaries in Alzheimer's disease via signaling to pericytes. Science 2019;365:eaav9518. doi: https://doi.org/10.1126/science.aav9518.
[11] Ding R, Hase Y, Ameen-Ali KE, Ndung'u M, Stevenson W, Barsby J, et al. Loss of capillary pericytes and the blood–brain barrier in white matter in poststroke and vascular dementias and Alzheimer's disease. Brain Pathol 2020;30:1087–101. doi: https://doi.org/10.1111/bpa.12888.
[12] Tsao C-C, Baumann J, Huang S-F, Kindler D, Schroeter A, Kachappilly N, et al. Pericyte hypoxia-inducible factor-1 (HIF-1) drives blood-brain barrier disruption and impacts acute ischemic stroke outcome. Angiogenesis 2021;24:823–42. doi: https://doi.org/10.1007/s10456-021-09796-4.
[13] Yao F, Luo Y, Liu Y-C, Chen Y-H, Li Y-T, Hu X-Y, et al. Imatinib inhibits pericyte-fibroblast transition and inflammation and promotes axon regeneration by blocking the PDGF-BB/PDGFRβ pathway in spinal cord injury. Inflammation and Regeneration 2022;42:44. doi: https://doi.org/10.1186/s41232-022-00223-9.
[14] Göritz C, Dias DO, Tomilin N, Barbacid M, Shupliakov O, Frisén J. A pericyte origin of spinal cord scar tissue. Science 2011;333:238–42. doi: https://doi.org/10.1126/science.1203165.
[15] Nakagomi T, Kubo S, Nakano-Doi A, Sakuma R, Lu S, Narita A, et al. Brain vascular pericytes following ischemia have multipotential stem cell activity to differentiate into neural and vascular lineage cells. Stem Cells 2015;33:1962–74. doi: https://doi.org/10.1002/stem.1977.
[16] O'Farrell FM, Mastitskaya S, Hammond-Haley M, Freitas F, Wah WR, Attwell D. Capillary pericytes mediate coronary no-reflow after myocardial ischaemia. Elife 2017;6:e29280. doi: https://doi.org/10.7554/eLife.29280.
[17] Dalkara T, Alarcon-Martinez L, Yemisci M. Pericytes in ischemic stroke. In: Birbrair A, editor. Pericyte Biology in Disease. Cham: Springer International Publishing; 2019. p. 189–213. doi: https://doi.org/10.1007/978-3-030-16908-4_9.
[18] Cao L, Zhou Y, Chen M, Li L, Zhang W. Pericytes for therapeutic approaches to ischemic stroke. Front Neurosci 2021;15:629297. doi: https://doi.org/10.3389/fnins.2021.629297.
[19] Li P, Wu Y, Hamlett ED, Goodwin AJ, Halushka PV, Carroll SL, et al. Suppression of Fli-1 protects against pericyte loss and cognitive deficits in Alzheimer's disease. Mol Ther 2022;30:1451–64. doi: https://doi.org/10.1016/j.ymthe.2022.01.023.
[20] Zhou W, Chen C, Shi Y, Wu Q, Gimple RC, Fang X, et al. Targeting glioma stem cell-derived pericytes disrupts the blood-tumor barrier and improves chemotherapeutic efficacy. Cell Stem Cell 2017;21:591–603.e4. doi: https://doi.org/10.1016/j.stem.2017.10.002.
[21] Valdor R, García-Bernal D, Riquelme D, Martinez CM, Moraleda JM, Cuervo AM, et al. Glioblastoma ablates pericytes antitumor immune function through aberrant up-regulation of chaperone-mediated autophagy. PNAS 2019;116:20655–65. doi: https://doi.org/10.1073/pnas.1903542116.
[22] Segura-Collar B, Garranzo-Asensio M, Herranz B, Hernández-SanMiguel E, Cejalvo T, Casas BS, et al. Tumor-derived pericytes driven by EGFR mutations govern the vascular and immune microenvironment of gliomas. Cancer Res 2021;81:2142–56. doi: https://doi.org/10.1158/0008-5472.CAN-20-3558.
[23] Geranmayeh MH, Rahbarghazi R, Farhoudi M. Targeting pericytes for neurovascular regeneration. Cell Commun Signaling 2019;17:26. doi: https://doi.org/10.1186/s12964-019-0340-8.
[24] Courtney J-M, Sutherland BA. Harnessing the stem cell properties of pericytes to repair the brain. Neural Regen Res 2020;15:1021–2. doi: https://doi.org/10.4103/1673-5374.270301.
[25] Birbrair A, Zhang T, Wang Z-M, Messi ML, Enikolopov GN, Mintz A, et al. Role of pericytes in skeletal muscle regeneration and fat accumulation. Stem Cells Dev 2013;22:2298–314. doi: https://doi.org/10.1089/scd.2012.0647.
[26] Birbrair A, Zhang T, Wang Z-M, Messi ML, Olson JD, Mintz A, et al. Type-2 pericytes participate in normal and tumoral angiogenesis. Am J Phys Cell Phys 2014;307:C25–38. doi: https://doi.org/10.1152/ajpcell.00084.2014.
[27] Sharma K, Zhang Y, Paudel KR, Kachelmeier A, Hansbro PM, Shi X. The emerging role of pericyte-derived extracellular vesicles in vascular and neurological health. Cells 2022;11:3108. doi: https://doi.org/10.3390/cells11193108.
[28] Fred DJ. Peptide sequences that target cytosolic proteins for lysosomal proteolysis. Trends Biochem Sci 1990;15:305–9. doi: https://doi.org/10.1016/0968-0004(90)90019-8.
[29] Kirchner P, Bourdenx M, Madrigal-Matute J, Tiano S, Diaz A, Bartholdy BA, et al. Proteome-wide analysis of chaperone-mediated autophagy targeting motifs. PLoS Biol 2019;17:e3000301. doi: https://doi.org/10.1371/journal.pbio.3000301.
[30] Cuervo AM, Dice JF. A receptor for the selective uptake and degradation of proteins by lysosomes. Science 1996;273:501–3. doi: https://doi.org/10.1126/science.273.5274.501.
[31] Bandyopadhyay U, Kaushik S, Varticovski L, Cuervo AM. The chaperone-mediated autophagy receptor organizes in dynamic protein complexes at the lysosomal membrane. Mol Cell Biol 2008;28:5747–63. doi: https://doi.org/10.1128/MCB.02070-07.
[32] Kaushik S, Cuervo AM. The coming of age of chaperone-mediated autophagy. Nat Rev Mol Cell Biol 2018;19:365–81. doi: https://doi.org/10.1038/s41580-018-0001-6.
[33] Gomez-Sintes R, Xin Q, Jimenez-Loygorri JI, McCabe M, Diaz A, Garner TP, et al. Targeting retinoic acid receptor alpha-corepressor interaction activates chaperone-mediated autophagy and protects against retinal degeneration. Nat Commun 2022;13:4220. doi: https://doi.org/10.1038/s41467-022-31869-1.
[34] Valdor R, Martinez-Vicente M. The role of chaperone-mediated autophagy in tissue homeostasis and disease pathogenesis. Biomedicines 2024;12:257. doi: https://doi.org/10.3390/biomedicines12020257.
[35] Vitale E, Perveen S, Rossin D, Lo Iacono M, Rastaldo R, Giachino C. Role of chaperone-mediated autophagy in ageing biology and rejuvenation of stem cells. Front Cell Dev Biol 2022;10:912470. doi: https://doi.org/10.3389/fcell.2022.912470.
[36] Zhang H, Tian Y, Ma S, Ji Y, Wang Z, Xiao P, et al. Chaperone-mediated autophagy in brain injury: a double-edged sword with therapeutic potentials. Mol Neurobiol 2024;61:10671–83. doi: https://doi.org/10.1007/s12035-024-04230-4.
[37] Kiffin R, Christian C, Knecht E, Cuervo AM. Activation of chaperone-mediated autophagy during oxidative stress. Mol Biol Cell 2004;15:4829–40. doi: https://doi.org/10.1091/mbc.E04-06-0477.
[38] Hubbi ME, Hu H, Kshitiz AI, Levchenko A, Semenza GL. Chaperone-mediated autophagy targets hypoxia-inducible factor-1α (HIF-1α) for lysosomal degradation. J Biol Chem 2013;288:10703–14. doi: https://doi.org/10.1074/jbc.M112.414771.
[39] Valdor R, Mocholi E, Botbol Y, Guerrero-Ros I, Chandra D, Koga H, et al. Chaperone-mediated autophagy regulates T cell responses through targeted degradation of negative regulators of T cell activation. Nat Immunol 2014;15:1046–54. doi: https://doi.org/10.1038/ni.3003.
[40] Jafari M, Macho-González A, Diaz A, Lindenau K, Santiago-Fernández O, Zeng M, et al. Calorie restriction and calorie-restriction mimetics activate chaperone-mediated autophagy. Proc Natl Acad Sci 2024;121:e2317945121. doi: https://doi.org/10.1073/pnas.2317945121.
[41] Cuervo AM, Dice JF. Age-related decline in chaperone-mediated autophagy*. J Biol Chem 2000;275:31505–13. doi: https://doi.org/10.1074/jbc.M002102200.
[42] Massey AC, Kaushik S, Sovak G, Kiffin R, Cuervo AM. Consequences of the selective blockage of chaperone-mediated autophagy. PNAS 2006;103:5805–10. doi: https://doi.org/10.1073/pnas.0507436103.
[43] Rodriguez-Navarro JA, Kaushik S, Koga H, Dall'Armi C, Shui G, Wenk MR, et al. Inhibitory effect of dietary lipids on chaperone-mediated autophagy. Proc Natl Acad Sci U S A 2012;109:E705–14. doi: https://doi.org/10.1073/pnas.1113036109.
[44] Xilouri M, Brekk OR, Landeck N, Pitychoutis PM, Papasilekas T, Papadopoulou-Daifoti Z, et al. Boosting chaperone-mediated autophagy in vivo mitigates α-synuclein-induced neurodegeneration. Brain 2013;136:2130–46. doi: https://doi.org/10.1093/brain/awt131.
[45] Schneider JL, Villarroya J, Diaz-Carretero A, Patel B, Urbanska AM, Thi MM, et al. Loss of hepatic chaperone-mediated autophagy accelerates proteostasis failure in aging. Aging Cell 2015;14:249–64. doi: https://doi.org/10.1111/acel.12310.
[46] Andrade-Tomaz M, de Souza I, Rocha CRR, Gomes LR. The role of chaperone-mediated autophagy in cell cycle control and its implications in cancer. Cells 2020;9:2140. doi: https://doi.org/10.3390/cells9092140.
[47] Bourdenx M, Martín-Segura A, Scrivo A, Rodriguez-Navarro JA, Kaushik S, Tasset I, et al. Chaperone-mediated autophagy prevents collapse of the neuronal metastable proteome. Cell 2021;184:2696–2714.e25. doi: https://doi.org/10.1016/j.cell.2021.03.048.
[48] Wang F, Tasset I, Cuervo AM, Muller S. In vivo remodeling of altered autophagy-lysosomal pathway by a phosphopeptide in lupus. Cells 2020;9:2328. doi: https://doi.org/10.3390/cells9102328.
[49] Madrigal-Matute J, de Bruijn J, van Kuijk K, Riascos-Bernal DF, Diaz A, Tasset I, et al. Protective role of chaperone-mediated autophagy against

atherosclerosis. Proc Natl Acad Sci 2022;119:e2121133119. doi: https://doi.org/10.1073/pnas.2121133119.
[50] Retnakumar SV, Geesala R, Bretin A, Tourneur-Marsille J, Ogier-Denis E, Maretzky T, et al. Targeting the endo-lysosomal autophagy pathway to treat inflammatory bowel diseases. J Autoimmun 2022;128:102814. doi: https://doi.org/10.1016/j.jaut.2022.102814.
[51] Ghosh R, Gillaspie JJ, Campbell KS, Symons JD, Boudina S, Pattison JS. Chaperone-mediated autophagy protects cardiomyocytes against hypoxic-cell death. Am J Phys Cell Phys 2022;323:C1555–75. doi: https://doi.org/10.1152/ajpcell.00369.2021.
[52] Fleming A, Bourdenx M, Fujimaki M, Karabiyik C, Krause GJ, Lopez A, et al. The different autophagy degradation pathways and neurodegeneration. Neuron 2022;110:935–66. doi: https://doi.org/10.1016/j.neuron.2022.01.017.
[53] Jeong Y-J, Lee K-H, Woo J, Kim JY, Lee C-H, Yoo C-G. Downregulation of lysosome-associated membrane protein-2A contributes to the pathogenesis of COPD. COPD 2023;18:289–303. doi: https://doi.org/10.2147/COPD.S378386.
[54] Wu J, Han Y, Xu H, Sun H, Wang R, Ren H, et al. Deficient chaperone-mediated autophagy facilitates LPS-induced microglial activation via regulation of the p300/NF-κB/NLRP3 pathway. Sci Adv 2023;9:eadi8343. doi: https://doi.org/10.1126/sciadv.adi8343.
[55] Zheng Y, Peng L, Jiang G, Zhou J, Yang S, Bai L, et al. Activation of chaperone-mediated autophagy exerting neuroprotection effect on intracerebral hemorrhage-induced neuronal injury by targeting Lamp2a. Exp Neurol 2024;382:114986. doi: https://doi.org/10.1016/j.expneurol.2024.114986.
[56] Xu Y, Zhang Y, García-Cañaveras JC, Guo L, Kan M, Yu S, et al. Chaperone-mediated autophagy regulates the pluripotency of embryonic stem cells. Science 2020;369:397–403. doi: https://doi.org/10.1126/science.abb4467.
[57] Dong S, Wang Q, Kao Y-R, Diaz A, Tasset I, Kaushik S, et al. Chaperone-mediated autophagy sustains haematopoietic stem-cell function. Nature 2021;591:117–23. doi: https://doi.org/10.1038/s41586-020-03129-z.
[58] Kaushik S, Juste YR, Lindenau K, Dong S, Macho-González A, Santiago-Fernández O, et al. Chaperone-mediated autophagy regulates adipocyte differentiation. Sci Adv 2022;8:eabq2733. doi: https://doi.org/10.1126/sciadv.abq2733.
[59] Jafari M, McCabe M, Cuervo AM. Chaperone-mediated autophagy: mechanisms and physiological relevance. Curr Opin Physiol 2022;30:100597. doi: https://doi.org/10.1016/j.cophys.2022.100597.
[60] Auzmendi-Iriarte J, Otaegi-Ugartemendia M, Carrasco-Garcia E, Azkargorta M, Diaz A, Saenz-Antoñanzas A, et al. Chaperone-mediated autophagy controls proteomic and transcriptomic pathways to maintain glioma stem cell activity. Cancer Res 2022. doi: https://doi.org/10.1158/0008-5472.CAN-21-2161. canres .2161.2021.
[61] Auzmendi-Iriarte J, Matheu A. Intrinsic role of chaperone-mediated autophagy in cancer stem cell maintenance. Autophagy 2022:1–2. doi: https://doi.org/10.1080/15548627.2022.2069450.
[62] Salinas MD, Valdor R. Chaperone-mediated autophagy in pericytes: a key target for the development of new treatments against glioblastoma progression. Int J Mol Sci 2022;23:8886. doi: https://doi.org/10.3390/ijms23168886.
[63] Molina ML, García-Bernal D, Salinas MD, Rubio G, Aparicio P, Moraleda JM, et al. Chaperone-mediated autophagy ablation in pericytes reveals new glioblastoma prognostic markers and efficient treatment against tumor progression. Front Cell Dev Biol 2022;10:797945. doi: https://doi.org/10.3389/fcell.2022.797945.
[64] Oishi K, Kamiyashiki T, Ito Y. Isometric contraction of microvascular pericytes from mouse brain parenchyma. Microvasc Res 2007;73:20–8. doi: https://doi.org/10.1016/j.mvr.2006.08.004.
[65] Valdor R, García-Bernal D, Bueno C, Ródenas M, Moraleda JM, Macian F, et al. Glioblastoma progression is assisted by induction of immunosuppressive function of pericytes through interaction with tumor cells. Oncotarget 2017;8:68614–26. doi: https://doi.org/10.18632/oncotarget.19804.
[66] García-Bernal D, García-Arranz M, García-Guillén AI, García-Hernández AM, Blanquer M, García-Olmo D, et al. Exofucosylation of adipose mesenchymal stromal cells alters their secretome profile. Front Cell Dev Biol 2020;8:584074. doi: https://doi.org/10.3389/fcell.2020.584074.
[67] García-Bernal D, Blanquer M, Martínez CM, García-Guillén AI, García-Hernández AM, Carmen Algueró M, et al. Enforced mesenchymal stem cell tissue colonization counteracts immunopathology. Npj Regen Med 2022;7:1–16. doi: https://doi.org/10.1038/s41536-022-00258-z.
[68] Bueno C, Ramirez C, Rodríguez-Lozano FJ, Tabarés-Seisdedos R, Rodenas M, Moraleda JM, et al. Human adult periodontal ligament-derived cells integrate and differentiate after implantation into the adult mammalian brain. Cell Transplant 2013;22:2017–28. doi: https://doi.org/10.3727/096368912X657305.
[69] Bueno C, Martínez-Morga M, Martínez S. Non-proliferative neurogenesis in human periodontal ligament stem cells. Sci Rep 2019;9:18038. doi: https://doi.org/10.1038/s41598-019-54745-3.
[70] Rueda-Carrasco J, Martin-Bermejo MJ, Pereyra G, Mateo MI, Borroto A, Brosseron F, et al. SFRP1 modulates astrocyte-to-microglia crosstalk in acute and chronic neuroinflammation. EMBO Rep 2021;22:e51696. doi: https://doi.org/10.15252/embr.202051696.
[71] Luengo-Gil G, Calvo MI, Martín-Villar E, Águila S, Bohdan N, Antón AI, et al. Antithrombin controls tumor migration, invasion and angiogenesis by inhibition of enteropeptidase. Sci Rep 2016;6:27544. doi: https://doi.org/10.1038/srep27544.
[72] Love MI, Huber W, Anders S. Moderated estimation of fold change and dispersion for RNA-seq data with DESeq2. Genome Biol 2014;15:550. doi: https://doi.org/10.1186/s13059-014-0550-8.
[73] Ihaka R, Gentleman R. R: A language for data analysis and graphics. J Comput Graph Stat 1996;5:299–314. doi: https://doi.org/10.2307/1390807.
[74] Binns D, Dimmer E, Huntley R, Barrell D, O'Donovan C, Apweiler R. QuickGO: a web-based tool for Gene Ontology searching. Bioinformatics 2009;25:3045–6. doi: https://doi.org/10.1093/bioinformatics/btp536.
[75] Huntley RP, Sawford T, Mutowo-Meullenet P, Shypitsyna A, Bonilla C, Martin MJ, et al. The GOA database: Gene Ontology annotation updates for 2015. Nucleic Acids Res 2015;43:D1057–63. doi: https://doi.org/10.1093/nar/gku1113.
[76] Kronstrand R, Forsman M, Roman M. Quantitative analysis of drugs in hair by UHPLC high resolution mass spectrometry. Forensic Sci Int 2018;283:9–15. doi: https://doi.org/10.1016/j.forsciint.2017.12.001.
[77] Pascovici D, Handler DCL, Wu JX, Haynes PA. Multiple testing corrections in quantitative proteomics: a useful but blunt tool. Proteomics 2016;16:2448–53. doi: https://doi.org/10.1002/pmic.201600044.
[78] Hall SM. The effect of injections of lysophosphatidyl choline into white matter of the adult mouse spinal cord. J Cell Sci 1972;10:535–46. doi: https://doi.org/10.1242/jcs.10.2.535.
[79] Birgbauer E, Rao TS, Webb M. Lysolecithin induces demyelination in vitro in a cerebellar slice culture system. J Neurosci Res 2004;78:157–66. doi: https://doi.org/10.1002/jnr.20248.
[80] Bonilla S, Silva A, Valdés L, Geijo E, García-Verdugo JM, Martínez S. Functional neural stem cells derived from adult bone marrow. Neuroscience 2005;133:85–95. doi: https://doi.org/10.1016/j.neuroscience.2005.02.019.
[81] Cunha MI, Su M, Cantuti-Castelvetri L, Müller SA, Schifferer M, Djannatian M, et al. Pro-inflammatory activation following demyelination is required for myelin clearance and oligodendrogenesis. J Exp Med 2020;217. doi: https://doi.org/10.1084/jem.20191390.
[82] Koga H, Martinez-Vicente M, Macian F, Verkhusha VV, Cuervo AM. A photoconvertible fluorescent reporter to track chaperone-mediated autophagy. Nat Commun 2011;2:386. doi: https://doi.org/10.1038/ncomms1393.
[83] Kronenberg HM. Developmental regulation of the growth plate. Nature 2003;423:332–6. doi: https://doi.org/10.1038/nature01657.
[84] Long F, Ornitz DM. Development of the endochondral skeleton. Cold Spring Harb Perspect Biol 2013;5:a008334. doi: https://doi.org/10.1101/cshperspect.a008334.
[85] Chesi A, Wagley Y, Johnson ME, Manduchi E, Su C, Lu S, et al. Genome-scale Capture C promoter interactions implicate effector genes at GWAS loci for bone mineral density. Nat Commun 2019;10:1260. doi: https://doi.org/10.1038/s41467-019-09302-x.
[86] Mossahebi-Mohammadi M, Quan M, Zhang J-S, Li X. FGF signaling pathway: a key regulator of stem cell pluripotency. Front Cell Dev Biol 2020;8. doi: https://doi.org/10.3389/fcell.2020.00079.
[87] Lee S, Remark LH, Josephson AM, Leclerc K, Lopez EM, Kirby DJ, et al. Notch-Wnt signal crosstalk regulates proliferation and differentiation of osteoprogenitor cells during intramembranous bone healing. Npj Regen Med 2021;6:1–10. doi: https://doi.org/10.1038/s41536-021-00139-x.
[88] Chidiac R, Angers S. Chapter Four - Wnt signaling in stem cells during development and cell lineage specification. In: Yamaguchi TP, Willert K, editors. Current Topics in Developmental Biology. Academic Press; 2023. p. 121–43. doi: https://doi.org/10.1016/bs.ctdb.2023.01.005.
[89] Almalki SG, Agrawal DK. Key transcription factors in the differentiation of mesenchymal stem cells. Differentiation 2016;92:41–51. doi: https://doi.org/10.1016/j.diff.2016.02.005.
[90] Collett G, Wood A, Alexander MY, Varnum BC, Boot-Handford RP, Ohanian V, et al. Receptor tyrosine kinase Axl modulates the osteogenic differentiation of pericytes. Circ Res 2003;92:1123–9. doi: https://doi.org/10.1161/01.RES.0000074881.56564.46.
[91] Ramine KM. Receptor kinase AXL is modulated in the osteogenic differentiation of human mesenchymal stromal cells on modified titanium implant surfaces. Journal of Stem Cell Res Ther 2014;04.
[92] Mitterberger MC, Lechner S, Mattesich M, Kaiser A, Probst D, Wenger N, et al. DLK1(PREF1) is a negative regulator of adipogenesis in CD105+/CD90+/CD34+/CD31−/FABP4− adipose-derived stromal cells from subcutaneous abdominal fat pats of adult women. Stem Cell Res 2012;9:35–48. doi: https://doi.org/10.1016/j.scr.2012.04.001.
[93] Nueda M-L, González-Gómez M-J, Rodríguez-Cano M-M, Monsalve E-M, Díaz-Guerra MJM, Sánchez-Solana B, et al. DLK proteins modulate NOTCH signaling to influence a brown or white 3T3-L1 adipocyte fate. Sci Rep 2018;8:16923. doi: https://doi.org/10.1038/s41598-018-35252-3.
[94] Hatzmann FM, Ejaz A, Wiegers GJ, Mandl M, Brucker C, Lechner S, et al. Quiescence, stemness and adipogenic differentiation capacity in human DLK1−/CD34+/CD24+ adipose stem/progenitor cells. Cells 2021;10:214. doi: https://doi.org/10.3390/cells10020214.
[95] Karamanos NK, Theocharis AD, Piperigkou Z, Manou D, Passi A, Skandalis SS, et al. A guide to the composition and functions of the extracellular matrix. FEBS J 2021;288:6850–912. doi: https://doi.org/10.1111/febs.15776.
[96] Shibahara T, Nakamura K, Wakisaka Y, Shijo M, Yamanaka K, Takashima M, et al. PDGFRβ-positive cell-mediated post-stroke remodeling of fibronectin and laminin α2 for tissue repair and functional recovery. J Cereb Blood Flow Metab 2022. doi: https://doi.org/10.1177/0271678X221145092.

[97] Carmeliet P, Dor Y, Herbert J-M, Fukumura D, Brusselmans K, Dewerchin M, et al. Role of HIF-1α in hypoxia-mediated apoptosis, cell proliferation and tumour angiogenesis. Nature 1998;394:485–90. doi: https://doi.org/10.1038/28867.
[98] Baumann J, Tsao C-C, Patkar S, Huang S-F, Francia S, Magnussen SN, et al. Pericyte, but not astrocyte, hypoxia inducible factor-1 (HIF-1) drives hypoxia-induced vascular permeability in vivo. Fluids Barriers CNS 2022;19:6. doi: https://doi.org/10.1186/s12987-021-00302-y.
[99] Shenoy AK, Jin Y, Luo H, Tang M, Pampo C, Shao R, et al. Epithelial-to-mesenchymal transition confers pericyte properties on cancer cells. J Clin Invest 2016;126:4174–86. doi: https://doi.org/10.1172/JCI86623.
[100] Etchevers HC, Vincent C, Douarin NML, F. Couly G. The cephalic neural crest provides pericytes and smooth muscle cells to all blood vessels of the face and forebrain. Development 2001;128:1059–68. doi: https://doi.org/10.1242/dev.128.7.1059.
[101] Miletich I, Sharpe PT. Neural crest contribution to mammalian tooth formation. Birth Defects Res C Embryo Today 2004;72:200–12. doi: https://doi.org/10.1002/bdrc.20012.
[102] Coura GS, Garcez RC, De Aguiar CBNM, Alvarez-Silva M, Magini RS, Trentin AG. Human periodontal ligament: a niche of neural crest stem cells. J Periodontal Res 2008;43:531–6. doi: https://doi.org/10.1111/j.1600-0765.2007.01065.x.
[103] Yamazaki T, Mukouyama Y. Tissue specific origin, development, and pathological perspectives of pericytes. Front Cardiovasc Med 2018;5:00078. doi: https://doi.org/10.3389/fcvm.2018.00078.
[104] Zhao J, Chen X, Song G, Zhang J, Liu H, Liu X. Uhrf1 controls the self-renewal versus differentiation of hematopoietic stem cells by epigenetically regulating the cell-division modes. Proc Natl Acad Sci 2017;114:E142–51. doi: https://doi.org/10.1073/pnas.1612967114.
[105] Xiang H, Yuan L, Gao X, Alexander PB, Lopez O, Lau C, et al. UHRF1 is required for basal stem cell proliferation in response to airway injury. Cell Discov 2017;3:1–15. doi: https://doi.org/10.1038/celldisc.2017.19.
[106] Yuan B, Liu Y, Yu X, Yin L, Peng Y, Gao Y, et al. FOXM1 contributes to taxane resistance by regulating UHRF1-controlled cancer cell stemness. Cell Death Dis 2018;9:1–11. doi: https://doi.org/10.1038/s41419-018-0631-9.
[107] Qi S, Li Y, Dai Z, Xiang M, Wang G, Wang L, et al. Uhrf1-mediated Tnf-α gene methylation controls proinflammatory macrophages in experimental colitis resembling inflammatory bowel disease. J Immunol 2019;203:3045–53. doi: https://doi.org/10.4049/jimmunol.1900467.
[108] Chaly Y, Blair HC, Smith SM, Bushnell DS, Marinov AD, Campfield BT, et al. Follistatin-like protein 1 regulates chondrocyte proliferation and chondrogenic differentiation of mesenchymal stem cells. Ann Rheum Dis 2015;74:1467–73. doi: https://doi.org/10.1136/annrheumdis-2013-204822.
[109] Li W, Alahdal M, Deng Z, Liu J, Zhao Z, Cheng X, et al. Molecular functions of FSTL1 in the osteoarthritis. Int Immunopharmacol 2020;83:106465. doi: https://doi.org/10.1016/j.intimp.2020.106465.
[110] Li W, Zhang L, Yin X, Ai H. The effects of follistatin on the differentiation of human bone marrow mesenchymal stem cells into neurons-like cells. Ann Clin Lab Sci 2020;50:3–12.
[111] Bradshaw AD, Sage EH. SPARC, a matricellular protein that functions in cellular differentiation and tissue response to injury. J Clin Invest 2001;107:1049–54.
[112] Trombetta JM, Bradshaw AD, Johnson RH. SPARC/Osteonectin functions to maintain homeostasis of the collagenous extracellular matrix in the periodontal ligament. J Histochem Cytochem 2010;58:871–9. doi: https://doi.org/10.1369/jhc.2010.956144.
[113] Alkabie S, Basivireddy J, Zhou L, Roskams J, Rieckmann P, Quandt JA. SPARC expression by cerebral microvascular endothelial cells in vitro and its influence on blood-brain barrier properties. J Neuroinflammation 2016;13:225. doi: https://doi.org/10.1186/s12974-016-0657-9.
[114] Cárdenas-León CG, Mäemets-Allas K, Klaas M, Lagus H, Kankuri E, Jaks V. Matricellular proteins in cutaneous wound healing. Front Cell Dev Biol 2022;10:1073320. doi: https://doi.org/10.3389/fcell.2022.1073320.
[115] Bhakuni T, Ali MF, Ahmad I, Bano S, Ansari S, Jairajpuri MA. Role of heparin and non heparin binding serpins in coagulation and angiogenesis: a complex interplay. Arch Biochem Biophys 2016;604:128–42. doi: https://doi.org/10.1016/j.abb.2016.06.018.
[116] Jaiswal RK, Varshney AK, Yadava PK. Diversity and functional evolution of the plasminogen activator system. Biomed Pharmacother 2018;98:886–98. doi: https://doi.org/10.1016/j.biopha.2018.01.029.
[117] Baumeier C, Escher F, Aleshcheva G, Pietsch H, Schultheiss H-P. Plasminogen activator inhibitor-1 reduces cardiac fibrosis and promotes M2 macrophage polarization in inflammatory cardiomyopathy. Basic Res Cardiol 2021;116:1. doi: https://doi.org/10.1007/s00395-020-00840-w.
[118] Jung M, Lord MS, Cheng B, Lyons JG, Alkhouri H, Hughes JM, et al. Mast cells produce novel shorter forms of perlecan that contain functional endorepellin. J Biol Chem 2013;288:3289–304. doi: https://doi.org/10.1074/jbc.M112.387811.
[119] Nakamura K, Ikeuchi T, Nara K, Rhodes CS, Zhang P, Chiba Y, et al. Perlecan regulates pericyte dynamics in the maintenance and repair of the blood–brain barrier. J Cell Biol 2019;218:3506–25. doi: https://doi.org/10.1083/jcb.201807178.
[120] Trout AL, Kahle MP, Roberts JM, Marcelo A, de Hoog L, Boychuk JA, et al. Perlecan domain-V enhances neurogenic brain repair after stroke in mice. Transl Stroke Res 2021;12:72–86. doi: https://doi.org/10.1007/s12975-020-00800-5.
[121] Hayes AJ, Farrugia BL, Biose IJ, Bix GJ, Melrose JP. A multi-functional, cell-instructive, matrix-stabilizing proteoglycan with roles in tissue development has relevance to connective tissue repair and regeneration. Front Cell Dev Biol 2022;10:856261. doi: https://doi.org/10.3389/fcell.2022.856261.
[122] Topalov NE, Mayr D, Scherer C, Chelariu-Raicu A, Beyer S, Hester A, et al. Actin beta-like 2 as a new mediator of proliferation and migration in epithelial ovarian cancer. Front Oncol 2021;11:713026. doi: https://doi.org/10.3389/fonc.2021.713026.
[123] Oelschläger C, Römisch J, Staubitz A, Stauss H, Leithäuser B, Tillmanns H, et al. Antithrombin III inhibits nuclear factor κB activation in human monocytes and vascular endothelial cells. Blood 2002;99:4015–20. doi: https://doi.org/10.1182/blood.V99.11.4015.
[124] Rezaie AR, Giri H. Antithrombin: an anticoagulant, anti-inflammatory and antibacterial serpin. J Thromb Haemost 2020;18:528–33. doi: https://doi.org/10.1111/jth.14724.
[125] Lamers D, Famulla S, Wronkowitz N, Hartwig S, Lehr S, Ouwens DM, et al. Dipeptidyl peptidase 4 is a novel adipokine potentially linking obesity to the metabolic syndrome. Diabetes 2011;60:1917–25. doi: https://doi.org/10.2337/db10-1707.
[126] Lin L, Sun W, Throesch B, Kung F, Decoster JT, Berner CJ, et al. DPP6 regulation of dendritic morphogenesis impacts hippocampal synaptic development. Nat Commun 2013;4:2270. doi: https://doi.org/10.1038/ncomms3270.
[127] Lin L, Long LK, Hatch MM, Hoffman DA. DPP6 domains responsible for its localization and function. J Biol Chem 2014;289:32153–65. doi: https://doi.org/10.1074/jbc.M114.578070.
[128] Malloy C, Ahern M, Lin L, Hoffman DA. Neuronal roles of the multifunctional protein dipeptidyl peptidase-like 6 (DPP6). Int J Mol Sci 2022;23:9184. doi: https://doi.org/10.3390/ijms23169184.
[129] Ito K, Suda T. Metabolic requirements for the maintenance of self-renewing stem cells. Nat Rev Mol Cell Biol 2014;15:243–56. doi: https://doi.org/10.1038/nrm3772.
[130] Georgila K, Vyrla D, Drakos E. Apolipoprotein A-I (ApoA-I), immunity, inflammation and cancer. Cancers 2019;11:1097. doi: https://doi.org/10.3390/cancers11081097.
[131] Fuente AGDL, Lange S, Silva ME, Gonzalez GA, Tempfer H, van Wijngaarden P, et al. Pericytes stimulate oligodendrocyte progenitor cell differentiation during CNS remyelination. Cell Rep 2017;20:1755–64. doi: https://doi.org/10.1016/j.celrep.2017.08.007.
[132] Gómez-de Frutos MC, Laso-García F, Diekhorst L, Otero-Ortega L, Fuentes B, Jolkkonen J, et al. Intravenous delivery of adipose tissue-derived mesenchymal stem cells improves brain repair in hyperglycemic stroke rats. Stem Cell Res Ther 2019;10:212. doi: https://doi.org/10.1186/s13287-019-1322-x.
[133] Zhang W, Pu H, Hu X, Shi Y, Leak RK, Anne Stetler R, et al. Poststroke intravenous transplantation of human mesenchymal stem cells improves brain repair dynamics and functional outcomes in aged mice. Stroke 2023;54:1088–98. doi: https://doi.org/10.1161/STROKEAHA.122.041507.
[134] Jacobs HIL, Van Boxtel MPJ, Jolles J, Verhey FRJ, Uylings HBM. Parietal cortex matters in Alzheimer's disease: an overview of structural, functional and metabolic findings. Neurosci Biobehav Rev 2012;36:297–309. doi: https://doi.org/10.1016/j.neubiorev.2011.06.009.
[135] Gautam J, Cao Y, Yao Y. Pericytic laminin maintains blood-brain barrier integrity in an age-dependent manner. Transl Stroke Res 2020;11:228–42. doi: https://doi.org/10.1007/s12975-019-00709-8.
[136] Zapata-Acevedo JF, García-Pérez V, Cabezas-Pérez R, Losada-Barragán M, Vargas-Sánchez K, González-Reyes RE. Laminin as a biomarker of blood–brain barrier disruption under neuroinflammation: a systematic review. Int J Mol Sci 2022;23:6788. doi: https://doi.org/10.3390/ijms23126788.
[137] Halder SK, Sapkota A, Milner R. The importance of laminin at the blood-brain barrier. Neural Regen Res 2023;18:2557. doi: https://doi.org/10.4103/1673-5374.373677.
[138] Zhang J, Huang J, Gu Y, Xue M, Qian F, Wang B, et al. Inflammation-induced inhibition of chaperone-mediated autophagy maintains the immunosuppressive function of murine mesenchymal stromal cells. Cell Mol Immunol 2021;18:1476–88. doi: https://doi.org/10.1038/s41423-019-0345-7.
[139] Benveniste EN. Cytokine actions in the central nervous system. Cytokine Growth Factor Rev 1998;9:259–75. doi: https://doi.org/10.1016/S1359-6101(98)00015-X.
[140] Corbin-Stein NJ, Childers GM, Webster JM, Zane A, Yang Y-T, Mudium N, et al. IFNγ drives neuroinflammation, demyelination, and neurodegeneration in a mouse model of multiple system atrophy. Acta Neuropathol Commun 2024;12:11. doi: https://doi.org/10.1186/s40478-023-01710-x.
[141] Hemmer K, Fransen L, Vanderstichele H, Vanmechelen E, Heuschling P. An in vitro model for the study of microglia-induced neurodegeneration: involvement of nitric oxide and tumor necrosis factor-α. Neurochem Int 2001;38:557–65. doi: https://doi.org/10.1016/S0197-0186(00)00119-4.
[142] Minghetti L. Cyclooxygenase-2 (COX-2) in inflammatory and degenerative brain diseases. J Neuropathol Exp Neurol 2004;63:901–10. doi: https://doi.org/10.1093/jnen/63.9.901.
[143] Block ML, Zecca L, Hong J-S. Microglia-mediated neurotoxicity: uncovering the molecular mechanisms. Nat Rev Neurosci 2007;8:57–69. doi: https://doi.org/10.1038/nrn2038.
[144] Supakul S, Yao K, Ochi H, Shimada T, Hashimoto K, Sunamura S, et al. Pericytes as a source of osteogenic cells in bone fracture healing. Int J Mol Sci 2019;20:1079. doi: https://doi.org/10.3390/ijms20051079.

[145] Issabekova A, Kudaibergen G, Sekenova A, Dairov A, Sarsenova M, Mukhlis S, et al. The therapeutic potential of pericytes in bone tissue regeneration. Biomedicines 2024;12:21. doi: https://doi.org/10.3390/biomedicines12010021.
[146] Polat S, Yazir Y, Duruksu G, Kiliç KC, Mert S, Gacar G, et al. Investigation of the differentiation potential of pericyte cells as an alternative source of mesenchymal stem cells. Acta Histochem 2024;126:152145. doi: https://doi.org/10.1016/j.acthis.2024.152145.
[147] Wong S-P, Rowley JE, Redpath AN, Tilman JD, Fellous TG, Johnson JR. Pericytes, mesenchymal stem cells and their contributions to tissue repair. Pharmacol Ther 2015;151:107–20. doi: https://doi.org/10.1016/j.pharmthera.2015.03.006.
[148] Xu J, Li D, Hsu C-Y, Tian Y, Zhang L, Wang Y, et al. Comparison of skeletal and soft tissue pericytes identifies CXCR4+ bone forming mural cells in human tissues. Bone Res 2020;8:1–14. doi: https://doi.org/10.1038/s41413-020-0097-0.
[149] Chua BA, Lennan CJ, Sunshine MJ, Dreifke D, Chawla A, Bennett EJ, et al. Hematopoietic stem cells preferentially traffic misfolded proteins to aggresomes and depend on aggrephagy to maintain protein homeostasis. Cell Stem Cell 2023;30:460–472.e6. doi: https://doi.org/10.1016/j.stem.2023.02.010.
[150] Gaceb A, Barbariga M, Özen I, Paul G. The pericyte secretome: Potential impact on regeneration. Biochimie 2018;155:16–25. doi: https://doi.org/10.1016/j.biochi.2018.04.015.
[151] Gaceb A, Özen I, Padel T, Barbariga M, Paul G. Pericytes secrete pro-regenerative molecules in response to platelet-derived growth factor-BB. J Cereb Blood Flow Metab 2018;38:45–57. doi: https://doi.org/10.1177/0271678X17719645.
[152] Uchiyama M, Nakamichi Y, Nakamura M, Kinugawa S, Yamada H, Udagawa N, et al. Dental pulp and periodontal ligament cells support osteoclastic differentiation. J Dent Res 2009;88:609–14. doi: https://doi.org/10.1177/0022034509340008.
[153] Kaushik S, Cuervo AM. Degradation of lipid droplet-associated proteins by chaperone-mediated autophagy facilitates lipolysis. Nat Cell Biol 2015;17:759–70. doi: https://doi.org/10.1038/ncb3166.
[154] Gong Y, Li Z, Zou S, Deng D, Lai P, Hu H, et al. Vangl2 limits chaperone-mediated autophagy to balance osteogenic differentiation in mesenchymal stem cells. Dev Cell 2021;56:2103–2120.e9. doi: https://doi.org/10.1016/j.devcel.2021.06.011.
[155] Pan W, Kastin AJ. Adipokines and the Blood-Brain Barrier. Peptides 2007;28:1317–30. doi: https://doi.org/10.1016/j.peptides.2007.04.023.
[156] Barbu A, Hamad OA, Lind L, Ekdahl KN, Nilsson B. The role of complement factor C3 in lipid metabolism. Mol Immunol 2015;67:101–7. doi: https://doi.org/10.1016/j.molimm.2015.02.027.
[157] Birbrair A, Zhang T, Files DC, Mannava S, Smith T, Wang Z-M, et al. Type-1 pericytes accumulate after tissue injury and produce collagen in an organ-dependent manner. Stem Cell Res Ther 2014;5:122. doi: https://doi.org/10.1186/scrt512.
[158] Chen J, Sivan U, Tan SL, Lippo L, De Angelis J, Labella R, et al. High-resolution 3D imaging uncovers organ-specific vascular control of tissue aging. Sci Adv 2021;7:eabd7819. doi: https://doi.org/10.1126/sciadv.abd7819.
[159] Kennedy BK, Berger SL, Brunet A, Campisi J, Cuervo AM, Epel ES, et al. Aging: a common driver of chronic diseases and a target for novel interventions. Cell 2014;159:709. doi: https://doi.org/10.1016/j.cell.2014.10.039.
[160] Lescat L, Herpin A, Mourot B, Véron V, Guiguen Y, Bobe J, et al. CMA restricted to mammals and birds: myth or reality? Autophagy 2018;14:1267–70. doi: https://doi.org/10.1080/15548627.2018.1460021.
[161] Lescat L, Véron V, Mourot B, Péron S, Chenais N, Dias K, et al. Chaperone-mediated autophagy in the light of evolution: insight from fish. Mol Biol Evol 2020;37:2887–99. doi: https://doi.org/10.1093/molbev/msaa127.
[162] Pant DC, Nazarko TY. Selective autophagy: the rise of the zebrafish model. Autophagy 2021;17:3297–305. doi: https://doi.org/10.1080/15548627.2020.1853382.
[163] Schnebert S, Vélez EJ, Goguet M, Dias K, Véron V, García-Pérez I, et al. Chaperone-mediated autophagy in fish: a key function amid a changing environment. Autophagy Rep 2024;3. doi: https://doi.org/10.1080/27694127.2024.2403956.